Available online at www.sciencedirect.com
ScienceDirect
Comput. Methods Appl. Mech. Engrg. 387 (2021) 114172
Computer methods in applied mechanics and engineering
www.elsevier.com/locate/cma

Efficient structural reliability analysis based on adaptive Bayesian support vector regression

Jinsheng Wang[a], Chenfeng Li[b,c], Guoji Xu[a,*], Yongle Li[a], Ahsan Kareem[d]

[a] *Department of Bridge Engineering, Southwest Jiaotong University, Chengdu, 610031, China*
[b] *Zienkiewicz Centre for Computational Engineering, College of Engineering, Swansea University, Swansea, SA1 8EN, UK*
[c] *Energy Safety Research Institute, College of Engineering, Swansea University, Swansea, SA1 8EN, UK*
[d] *NatHaz Modeling Laboratory, University of Notre Dame, Notre Dame, IN 46556, USA*

Received 13 January 2021; received in revised form 12 August 2021; accepted 2 September 2021
Available online xxxx

Abstract

To reduce the computational burden for structural reliability analysis involving complex numerical models, many adaptive algorithms based on surrogate models have been developed. Among the various surrogate models, the support vector machine for regression (SVR) which is derived from statistical learning theory has demonstrated superior performance to handle nonlinear problems and to avoid overfitting with excellent generalization. Therefore, to take the advantage of the desirable features of SVR, an Adaptive algorithm based on the Bayesian SVR model (ABSVR) is proposed in this study. In ABSVR, a new learning function is devised for the effective selection of informative sample points following the concept of the penalty function method in optimization. To improve the uniformity of sample points in the design of experiments (DoE), a distance constraint term is added to the learning function. Besides, an adaptive sampling region scheme is employed to filter out samples with weak probability density to further enhance the efficiency of the proposed algorithm. Moreover, a hybrid stopping criterion based on the error-based stopping criterion using the bootstrap confidence estimation is developed to terminate the active learning process to ensure that the learning algorithm stops at an appropriate stage. The proposed ABSVR is easy to implement since no embedded optimization algorithm nor iso-probabilistic transformation is required. The performance of ABSVR is evaluated using six numerical examples featuring different complexity, and the results demonstrate the superior performance of ABSVR for structural reliability analysis in terms of accuracy and efficiency.

Keywords: Structural reliability analysis; Adaptive surrogate models; Support vector regression; Bayesian inference; Learning function

1. Introduction

It is well recognized that the presence of uncertainties in practical engineering problems significantly affects the performance of structural systems, and uncertainty quantification with due consideration of these randomnesses are indispensable to the safety assessment, optimal design and serviceability maintenance of structures [1]. Hence, structural reliability theory which gives a rational treatment and provides a quantitative measurement of

* Corresponding author.
E-mail addresses: jinshengwangrjc@swjtu.edu.cn (J. Wang), c.f.li@swansea.ac.uk (C. Li), guoji.xu@swjtu.edu.cn (G. Xu), lele@swjtu.edu.cn (Y. Li), kareem@nd.edu (A. Kareem).

https://doi.org/10.1016/j.cma.2021.114172
0045-7825/

uncertainties has gained increasing attention in recent years. Structural reliability analysis aims to determine the probability of failure of a structural system with respect to some performance criterion in the presence of various uncertainties. Typically, the fundamental problem of structural reliability analysis can be mathematically defined as a multi-dimensional integral:

$$P_f = \text{Prob}[G(\boldsymbol{x}) \leq 0] = \int_{\Omega_f} f_{\boldsymbol{X}}(\boldsymbol{x}) d\boldsymbol{x} = \int_{\mathbb{R}^n} I_F(\boldsymbol{x}) f_{\boldsymbol{X}}(\boldsymbol{x}) d\boldsymbol{x} \tag{1}$$

where $\boldsymbol{x} = [x_1, x_2, \ldots, x_n]^T$ is a random vector with joint probability density function (PDF) $f_{\boldsymbol{X}}(\boldsymbol{x})$, representing the uncertainties arise from loading conditions, material properties, environmental factors, etc. $G(\boldsymbol{x})$ is the limit state function (LSF) defined in terms of $\boldsymbol{x}$, i.e. $G(\boldsymbol{x}) : \chi \subseteq \mathbb{R}^n \to \mathbb{R}, \boldsymbol{x} \mapsto g(\boldsymbol{x})$; Ω_f is the failure domain defined such that $\Omega_f = \{\boldsymbol{x} \in \chi : G(\boldsymbol{x}) \leq 0\}$, with its complementary set $\Omega_s = \{\boldsymbol{x} \in \chi : G(\boldsymbol{x}) > 0\}$ denotes the safe domain and $\Omega_0 = \{\boldsymbol{x} \in \chi : G(\boldsymbol{x}) = 0\}$ being defined as the limit state surface (LSS); and $I_F(\boldsymbol{x})$ is the indicator function given as:

$$I_F(\boldsymbol{x}) = I_{\Omega_f}(\boldsymbol{x}) = \begin{cases} 1 & \boldsymbol{x} \in \Omega_f \\ 0 & \boldsymbol{x} \in \Omega_s \end{cases} \tag{2}$$

The definition of failure probability in Eq. (1) is simple, but its calculation by direct integration is often intractable because the dimensionality of the integral is generally high and the LSS is of complicated geometry, especially for complex physical problems. The challenge of accurately computing this integral has led to the development of various reliability analysis methods, which can be broadly classified as approximation methods and sampling methods [2,3]. Specifically, the Monte Carlo simulation (MCS) is one of the most commonly used sampling methods because of its high accuracy, simplicity, and robustness. The MCS approach generates sample points using the distribution function associated with each random variable to estimate the failure probability, which is approximated as the ratio of failure realizations to the total number of evaluations:

$$P_f \approx \widehat{P}_f^{\text{MCS}} = \frac{1}{N} \sum_{i=1}^{N} I_F(\boldsymbol{x}^i) \tag{3}$$

where $\widehat{P}_f^{\text{MCS}}$ is the failure probability estimator of MCS, and $\left\{\boldsymbol{x}^{(i)}, i = 1, \ldots, N\right\}$ is the Monte Carlo population with a sample size of N. This estimator is asymptotically unbiased according to the central limit theorem, with its coefficient of variation being defined as:

$$\delta_{\text{MCS}} = \sqrt{\frac{1 - P_f}{N P_f}} \tag{4}$$

Thus, to ensure a small variation of the failure probability estimation, the required number of samples could be prohibitively high, i.e. the convergence rate is low $\left(\propto N^{-1/2}\right)$, especially for rare failure events entail demanding numerical models. Although advanced simulation methods such as importance sampling [4,5] and subset simulation [6,7] can greatly enhance the efficiency of MCS, the computational burden is still excessive for engineering problems. As an efficient alternative to the sampling methods, the approximation methods such as first-order reliability method (FORM) [8,9] and second-order reliability method (SORM) [10,11] are well-known for its simplicity and efficiency. In these methods, the performance function is usually approximated by a low-order (linear or quadratic) Taylor series expansion at the most probable point (MPP), where the isoprobabilistic transformation techniques are usually employed to transform the random variables from the physical space to the standard normal space [12], as illustrated in Fig. 1. Although they can provide reasonably accurate results with remarkable efficiency for some specific problems, the iterative MPP searching process may encounter non-convergence issues and the accuracy of the generated results cannot be guaranteed for problems with multiple MPPs and/or with highly nonlinear LSF. In this regard, the surrogate-based approximation methods, which can reach a good trade-off between efficiency and accuracy, are of particular interest in this paper.

The key idea of surrogate-based methods is to construct an easy-to-evaluate mathematical model to replace the original complex LSF, through which more simulation runs can be readily afforded [13]. Some of the representative surrogate modeling techniques include the response surface method (RSM) [14], the polynomial chaos expansion (PCE) [15] , the Kriging method [16], the radial basis function (RBF) [17], the support vector machine (SVM) (formulated in terms of classification (SVM) [18] or regression (SVR)) [19], the artificial neural

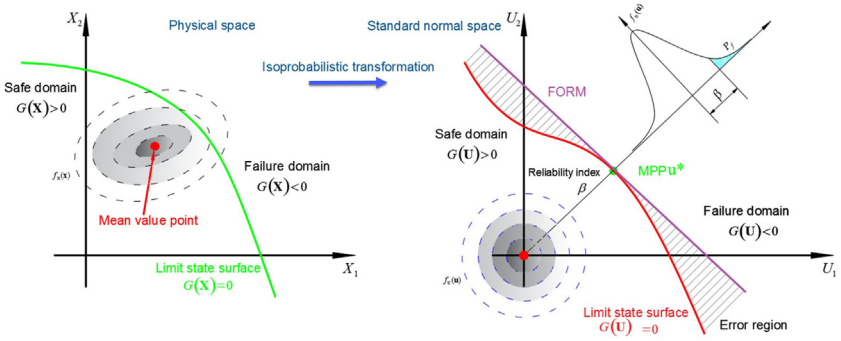

Fig. 1. Isoprobabilistic transformation from physical space to standard normal space. *Source:* adapted from [12].

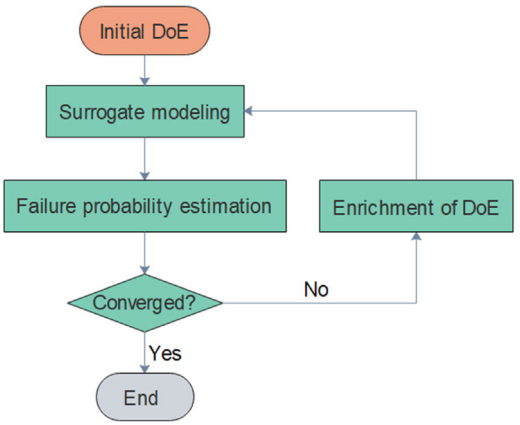

Fig. 2. The general procedure of surrogate-based active learning method for reliability analysis.

networks (ANN) [20] and more recently, the ensemble of surrogates [21], among others. A crucial issue for the construction of these surrogate models is the selection of an appropriate design of experiments (DoE), i.e. input–output training pairs. In general, there are two strategies for the DoE selection, namely the one-shot sampling schemes and the sequential sampling methods. The traditional one-shot sampling methods try to generate space-filling samples over the entire random space with a predefined sample size. In the context of structural reliability analysis, however, only regions near the LSS are of great interest and the appropriate number of samples is hard to determine *a priori* as too large or too small the sample size will both jeopardize the performance of surrogate-based methods. Therefore, various adaptive sampling schemes capable of exploiting the information contained in the constructed surrogate model have been developed to enrich the DoE in an iterative manner [22–24]. Reliability analysis methods empowered with adaptive sampling schemes are known as the active learning methods, where a preliminary surrogate model is established based on the initial DoE and then updated by sequentially enriching the DoE according to some judiciously selected learning functions. The general procedure of surrogate-based active learning methods for reliability analysis is illustrated in Fig. 2. By doing so, the efficiency of structural reliability analysis can significantly be improved without compromising accuracy.

Considering the superior performance of surrogate-based active learning methods, the development of effective learning algorithms is an active research topic in the structural reliability community. Bichon et al. [25] proposed an Efficient Global Reliability Analysis (EGRA) method, in which a learning function known as Expected Feasibility Function (EFF) was applied to select the new samples for the enrichment of DoE. This learning function indicates how well a point is expected to locate on the LSS, i.e. $G(\boldsymbol{x}) = 0$. The accuracy and efficiency of this method are demonstrated through numerical examples, yet its global approximation property may introduce redundant points with weak probability densities. To address this issue, an active learning method known as AK-MCS that combines

Kriging with crude MCS was developed by Echard et al. [26]. In AK-MCS, a large number of Monte Carlo populations are evaluated on the learning function U, and the one that minimizes U is selected as the best next point to be added to the DoE. This learning process enables the selection of samples with large probability density and assigns more weights to the points close to the LSS. Unlike the previous two adaptive algorithms where local prediction variance is used for the selection of new samples, the Markov chain simulation is employed in [27,28] to effective generate samples in the most likely failure regions, which enables the iterative refinement of the SVR model. Thanks to these (among others) pioneering works, new adaptive algorithms are emerging to further improve the computational accuracy and efficiency of structural reliability analysis. The related studies mainly focus on the development of effective DoE enrichment strategies to select new representative samples [29–31] and efficient stopping criteria to terminate the learning process at an appropriate stage [32–34]. In order to deal with rare failure events, the combination of surrogate models with advanced simulation methods has also gained increasingly more interest in recent years [35–37]. Due to the desirable features of adaptive algorithms, the adaption to other research fields such as design optimization [38,39] has also been explored. Readers are referred to [40] for a comprehensive review of the adaptive surrogate-based methods.

However, it is noted that most of the existing active learning methods are developed based on the Kriging model, where the error at unknown points can be empirically measured by the Kriging variance. Thus, the use of these learning algorithms to other surrogate models is not directly applicable unless additional effort such as bootstrap resampling strategy [41] or k fold cross-validation [42] is employed to get the prediction variance, which is a cumbersome process. To address this issue, several studies have been devoted to obtaining the variance in a more effective way, among which the Bayesian inference framework introduced in [43–45] has shown promising potential to establish a probabilistic interpretation of the surrogate models and to allow automatic adjustment of the kernel and regularization parameters to their near-optimal values [46]. From a weight-space perspective, the evidence framework [44] was applied to develop an alternative Bayesian interpretation of SVM for classification problems in [47] and regression problems in [48]. Following a similar idea, a probabilistic framework for SVR was proposed in [49], which enables the value of the hyperparameter to be determined by the Bayesian approach and the variance of the prediction to be derived from the Bayesian rule. More recently, Bayesian SVR models using different loss functions have been presented in [50–52] to further embrace the desirable features of the Bayesian inference framework. Similar to the Kriging model, the Bayesian SVR are capable of providing probabilistic prediction at a new point. Therefore, the ideas underlying Kriging-based active learning algorithms can readily be adapted to the Bayesian induced surrogate models [52].

Unlike models such as ANN and PCE which apply the principle of empirical risk minimization to mimic a true model, the SVR model is developed in the field of statistical learning theory and has revealed superior performance to handle nonlinear problems and avoid overfitting with good generalization ability. In this regard, the adaptive algorithm based on Bayesian SVR is expected to be well-suited for structural reliability analysis. In this paper, a novel Adaptive Bayesian SVR method (ABSVR) that combines with sampling region scheme and hybrid stopping criterion is proposed for efficient reliability analysis with high accuracy. Following the concept of the penalty function method in optimization, a new sampling-based learning function (SLF) is devised for the effective selection of informative sample points, e.g. points close to the LSS in critical regions with significant contribution to the failure probability. To improve the uniformity of sample points in the DoE, a distance constraint term is added to the learning function. Besides, the adaptive sampling region scheme [53] originally developed for Kriging-based approaches is adapted here to filter out sample points in regions with weak probability density, in that the samples in these regions have a negligible effect on the failure probability evaluation. In this way, the computational efficiency of ABSVR can be enhanced by using a set of important samples. Moreover, a hybrid stopping criterion based on the bootstrap confidence estimation (BCE) proposed in [34] is developed to terminate the active learning process, ensuring that the learning algorithm stops at an appropriate stage. The proposed ABSVR is easy to implement since no embedded optimization algorithm nor iso-probabilistic transformation is required.

The rest of this paper is organized as follows. The basic principle of Bayesian SVR models is introduced in Section 2. Section 3 recalls two advanced schemes for adaptive algorithms, namely the adaptive sampling region scheme and the error-based stopping criterion. Section 4 presents the detailed derivation of the new learning function, and the hybrid stopping criterion is proposed in Section 5. The implementation procedure of the proposed ABSVR is summarized in Section 6. The accuracy, efficiency, and robustness of ABSVR are illustrated in Section 7 using several numerical examples. Finally, concluding remarks are drawn in Section 8.

2. Basic theory of Bayesian support vector regression

In this section, the basic theory of Bayesian support vector regression (BSVR) initially proposed in [50–52] is briefly introduced, with particular emphasis on the BSVR models established with two loss functions, namely the square loss function (SLF) and the ε-insensitive square loss function (EISLF), which are respectively given as:

$$\ell_{\mathrm{SLF}}(\delta) = \frac{1}{2}\delta^2 \tag{5}$$

$$\ell_{\mathrm{EISLF}}(\delta) = \begin{cases} 0, & \text{if } |\delta| \le \varepsilon \\ \frac{1}{2}(|\delta| - \varepsilon)^2, & \text{otherwise} \end{cases} \tag{6}$$

where ε (with $\varepsilon > 0$) is an unknown parameter to be determined. It is noted that a soft insensitive loss function (SILF) is presented in [50] for the same purpose.

2.1. BayesIan inference framework

In the Bayesian framework, the regression model $h(\boldsymbol{x}_i)$ is assumed as a stationary Gaussian process with unknown mean b, and the covariance between two outputs is defined as:

$$\mathrm{Cov}\left[h(\boldsymbol{x}_i), h(\boldsymbol{x}_j)\right] = k(\boldsymbol{x}_i, \boldsymbol{x}_j) = \prod_{k=1}^{n} \exp\left(-\theta_k \left(x_i^k - x_j^k\right)^2\right) \tag{7}$$

where $\boldsymbol{\theta} = [\theta_1, \theta_2, \ldots, \theta_n]^T$ are the corresponding hyperparameters. The Gaussian kernel is adopted here because this kernel provides good performance under general smoothness assumptions, especially if no additional knowledge of the data is available [54]. Nevertheless, any other type of kernel functions such as those introduced in [55] may also be used.

Given a set of training sample pairs, i.e. $\mathcal{D} = \{(\boldsymbol{x}_i, y_i) \mid i = 1, \ldots, N, \boldsymbol{x}_i \in \mathbb{R}^n, y_i \in \mathbb{R}\}$, let $\boldsymbol{\chi}$ denote all the hyperparameters in the regression model and $\mathcal{H} = [h(\boldsymbol{x}_1), h(\boldsymbol{x}_2), \ldots, h(\boldsymbol{x}_N)]^T$. According to the Bayes' theorem,

$$\mathcal{P}(\mathcal{H} \mid \mathcal{D}, \boldsymbol{\chi}) = \frac{\mathcal{P}(\mathcal{D} \mid \mathcal{H}, \boldsymbol{\chi})\mathcal{P}(\mathcal{H} \mid \boldsymbol{\chi})}{\mathcal{P}(\mathcal{D} \mid \boldsymbol{\chi})} \tag{8}$$

where $\mathcal{P}(\mathcal{D} \mid \mathcal{H}, \boldsymbol{\chi})$ is the likelihood function of the given data set $\mathcal{D}$, $\mathcal{P}(\mathcal{H} \mid \boldsymbol{\chi})$ denotes the prior probability of $\mathcal{H}$, and $\mathcal{P}(\mathcal{D} \mid \boldsymbol{\chi})$ is a normalizing constant. The posterior probability $\mathcal{P}(\mathcal{H} \mid \mathcal{D}, \boldsymbol{\chi})$ of $\mathcal{H}$ can be derived as [51,52]:

$$\mathcal{P}(\mathcal{H} \mid \mathcal{D}, \boldsymbol{\chi}) = \frac{1}{\mathcal{Z}} \exp\left(-\eta \sum_{i=1}^{N} \ell(y_i - h(\boldsymbol{x}_i)) - \frac{1}{2}(\mathcal{H} - \boldsymbol{b})^T \mathcal{R}^{-1} (\mathcal{H} - \boldsymbol{b})\right) \tag{9}$$

where $\mathcal{Z} = \int \exp(-(\eta \sum_{i=1}^{N} \ell(y_i - h(\boldsymbol{x}_i)) + \frac{1}{2}\mathcal{H}^T \mathcal{R}^{-1}\mathcal{H}))d\mathcal{H}$, η is a constant value greater than zero, $\mathcal{R} \in \mathbb{R}^{N \times N}$ is the covariance matrix with the ijth element express as $\mathcal{R}_{ij} = \mathrm{Cov}\left[h(\boldsymbol{x}_i), h(\boldsymbol{x}_j)\right], i, j = 1, 2, \ldots, N$, and $\boldsymbol{b} = [b, \ldots, b] \in \mathbb{R}^{N \times 1}$.

Thus, the maximum *a posteriori* estimate of $\mathcal{P}(\mathcal{H} \mid \mathcal{D}, \boldsymbol{\chi})$ is equivalent to the following optimization problem:

$$\min_{\mathcal{H}} \eta \sum_{i=1}^{N} \ell(y_i - h(\boldsymbol{x}_i)) + \frac{1}{2}(\mathcal{H} - \boldsymbol{b})^T \mathcal{R}^{-1} (\mathcal{H} - \boldsymbol{b}) \tag{10}$$

2.2. BayesIan support vector regression

Introducing the SLF defined in Eq. (5) into the optimization problem described in Eq. (10), the optimal value $\widehat{\mathcal{H}}$ of $\mathcal{H}$ using SLF can be obtained as [51]:

$$\widehat{\mathcal{H}}_{\mathrm{SLF}} = \mathcal{R}(\mathcal{R} + \boldsymbol{I}/\eta)^{-1}\mathcal{Y} + \boldsymbol{b} \tag{11}$$

where $\boldsymbol{I} \in \mathbb{R}^{N\times N}$ is an identity matrix, and $\mathcal{Y} = \{y_1, \ldots, y_N\}^{\mathrm{T}}$. In the Bayesian framework, the hyperparameters of the model can be obtained by solving the following minimization problem:

$$\min_{\boldsymbol{\chi}} -\ln(\mathcal{P}(\mathcal{D} \mid \boldsymbol{\chi})) = \eta \sum_{i=1}^{N} \ell_{\mathrm{SLF}}\left(y_i - \widehat{h}\left(\boldsymbol{x}_i\right)\right) + \frac{1}{2}\boldsymbol{\beta}^T \mathcal{R}\boldsymbol{\beta} + \frac{1}{2}\ln|\boldsymbol{I} + \eta\mathcal{R}| + \frac{N}{2}\ln(\frac{2\pi}{\eta}) \tag{12}$$

where $\boldsymbol{\beta} = [\beta_1, \ldots, \beta_N]^{\mathrm{T}} = (\mathcal{R} + \boldsymbol{I}/\eta)^{-1}\mathcal{Y}$, and $\mathcal{P}(\mathcal{D} \mid \boldsymbol{\chi})$ is the Bayesian model evidence.

Similarly, the optimal value $\widehat{\mathcal{H}}$ of $\mathcal{H}$ using EISLF in Eq. (6) can be facilitated in the context of Lagrange duality, which leads to the following regression function [51]:

$$\widehat{\mathcal{H}}_{\mathrm{EISLF}} = \mathcal{R}\left(\boldsymbol{\alpha} - \boldsymbol{\alpha}^*\right) + \boldsymbol{b} \tag{13}$$

where $\boldsymbol{\alpha}^* = \left(\alpha_1^*, \ldots, \alpha_N^*\right)^{\mathrm{T}}, \boldsymbol{\alpha} = (\alpha_1, \ldots, \alpha_N)^{\mathrm{T}}$ are the Lagrangian multipliers, and support vectors are defined as the sample points with $\alpha_i - \alpha_i^* \neq 0$. The hyperparameters are obtained by solving the following minimization problem:

$$\min_{\boldsymbol{\chi}} -\ln(\mathcal{P}(\mathcal{D} \mid \boldsymbol{\chi})) = \eta \sum_{i=1}^{N} \ell_{\mathrm{EISLF}}\left(y_i - \widehat{h}\left(\boldsymbol{x}_i\right)\right) + \frac{1}{2}\left(\boldsymbol{\alpha} - \boldsymbol{\alpha}^*\right)^T \mathcal{R}\left(\boldsymbol{\alpha} - \boldsymbol{\alpha}^*\right) + \frac{1}{2}\ln|\mathcal{L}| + N\ln(2\varepsilon + \sqrt{\frac{2\pi}{\eta}}) \tag{14}$$

where $\mathcal{L} = \mathbf{I} + \eta\boldsymbol{\Lambda}\mathcal{R}$, and $\boldsymbol{\Lambda}$ is a diagonal matrix with its entry equal to 1 for support vectors and zero otherwise.

2.3. Probabilistic prediction of BSVR

Once the optimal BSVR model is established following the abovementioned procedures, the posterior distribution of $h(\boldsymbol{x})$ is a Gaussian distribution under the Gaussian process assumption [50,51]. For the SLF-based BSVR model, the prediction mean $\widehat{\mu}_{\hat{g}}(\boldsymbol{x})$ and prediction variance $\widehat{\sigma}_{\hat{g}}^2(\boldsymbol{x})$ are obtained as:

$$\widehat{\mu}_{\hat{g}}(\boldsymbol{x}) = \boldsymbol{k}(\boldsymbol{x}, \boldsymbol{X})(\mathcal{R} + \boldsymbol{I}/\eta)^{-1}\mathcal{Y} + b \tag{15}$$

$$\widehat{\sigma}_{\hat{g}}^2(\boldsymbol{x}) = k(\boldsymbol{x}, \boldsymbol{x}) - \boldsymbol{k}(\boldsymbol{x}, \boldsymbol{X})(\mathcal{R} + \boldsymbol{I}/\eta)^{-1}\boldsymbol{k}(\boldsymbol{X}, \boldsymbol{x}) \tag{16}$$

where $\boldsymbol{X} = \{\boldsymbol{x}_1, \ldots, \boldsymbol{x}_N\}^{\mathrm{T}}$, and $\boldsymbol{k}(\boldsymbol{x}, \boldsymbol{X}) = \boldsymbol{k}(\boldsymbol{X}, \boldsymbol{x})^{\mathrm{T}} = [k(\boldsymbol{x}_1, \boldsymbol{x}), \ldots, k(\boldsymbol{x}_N, \boldsymbol{x})]^{\mathrm{T}}$ is the covariance vector between $h(\boldsymbol{x})$ at a new point $\boldsymbol{x}$ and those in $\mathcal{H}$ evaluated at $\boldsymbol{X}$, which can be calculated from Eq. (7). For the EISLF-based BSVR model, the $\widehat{\mu}_{\hat{g}}(\boldsymbol{x})$ and $\widehat{\sigma}_{\hat{g}}^2(\boldsymbol{x})$ are obtained as:

$$\widehat{\mu}_{\hat{g}}(\boldsymbol{x}) = \boldsymbol{k}(\boldsymbol{x}, \boldsymbol{X})\mathcal{R}^{-1} = \sum_{j=1}^{m}\left(\alpha_j - \alpha_j^*\right)\boldsymbol{k}\left(\boldsymbol{x}, \boldsymbol{x}_j\right) + b \tag{17}$$

$$\widehat{\sigma}_{\hat{g}}^2(\boldsymbol{x}) = k(\boldsymbol{x}, \boldsymbol{x}) - \boldsymbol{k}_m(\boldsymbol{x}, \boldsymbol{X}_m)\left(\mathcal{R}_m + \boldsymbol{I}_m/\eta\right)^{-1}\boldsymbol{k}_m(\boldsymbol{X}_m, \boldsymbol{x}) \tag{18}$$

where $\boldsymbol{k}_m(\boldsymbol{x}, \boldsymbol{X}_m)$ and $\mathcal{R}_m$ are the subsets of $\boldsymbol{k}(\boldsymbol{x}, \boldsymbol{X})$ and $\mathcal{R}$, respectively, with their elements evaluated at the support vectors $\boldsymbol{X}_m$.

The BSVR models are established following the above procedures, and more information regarding the derivation of BSVR can be found in [50–52]. It is noted that the Bayesian SVR model using the square loss function leads to a formulation similar to the least-square SVR with the predictor being expressed in terms of all training points, and the problem to solve is equivalent to the noisy Kriging in theory. In fact, the equivalence between the least-square SVR and the ordinary Kriging has been demonstrated in [56]. The probabilistic prediction parameters $\widehat{\mu}(\boldsymbol{x})$ and $\widehat{\sigma}^2(\boldsymbol{x})$ can now be employed to devise active learning algorithms for efficient reliability analysis based on the BSVR model, which is the main focus of this paper and will be explained in the following sections.

3. The advanced schemes for adaptive algorithm

The critical role of learning function in adaptive algorithms is well-recognized, while the influence of effective sampling regions for the selection of sample points and the error-based stopping criteria for the termination of the learning process did not draw too much attention until recently. Indeed, an improper sampling scheme may introduce samples with weak probability densities that make barely any contribution to the failure probability, whereas

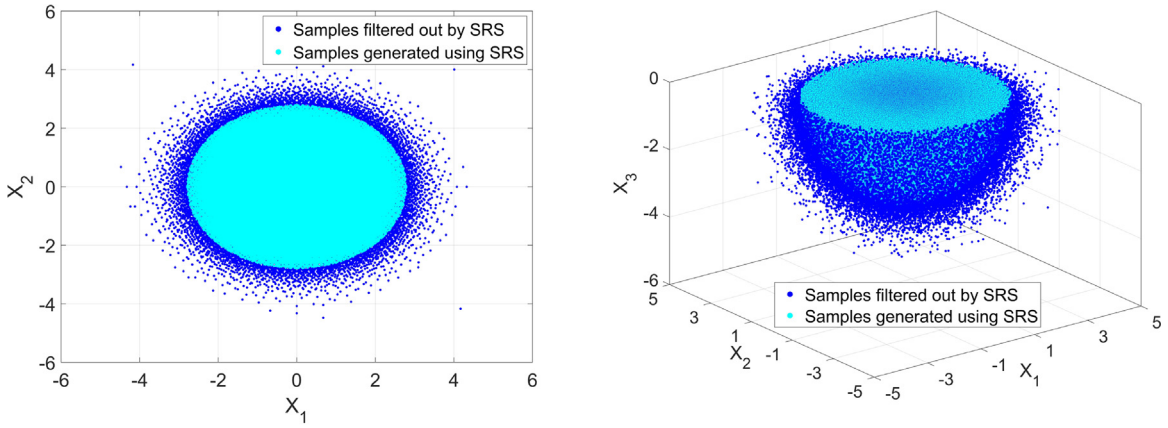

Fig. 3. Schematic illustration of the SRS with $p_t^{(i)} = 0.1$ and $\alpha = 0.2$: (a) a 2D case; (b) a 3D case (only half of the ball is shown). (For interpretation of the references to color in this figure, please refer to the web version of this article.)

inadequate selection of stopping criterion may lead to inaccurate estimation of the failure probability or results in high computational cost because of unnecessary calls to the performance function. Both can adversely affect the performance of an adaptive algorithm. To address these issues, several sampling region schemes (SRS) [53,57] and error-based stopping criteria (ESC) [32–34] have been proposed for effective reliability analysis. In this study, the sampling region scheme presented in [53] and the ESC using bootstrap confidence estimation (BCE) [34] will be integrated into the proposed method, namely the ABSVR.

3.1. Adaptive sampling region scheme

In the adaptive SRS, the region with the probability density larger than a threshold is progressively updated in the learning process, rather than fixing the sampling region in a predefined domain, which is given as [53]:

$$\hat{\Omega}_{(i)} = \left\{ \forall \boldsymbol{x} : f_{\boldsymbol{X}}(\boldsymbol{x}) > p_t^{(i)} \right\} \quad (i = 1, 2, \ldots) \tag{19}$$

where $p_t^{(i)}$ is the threshold value of the probability density in the ith iteration, and can be determined according to the following equation:

$$P\left\{ f_{\boldsymbol{X}}(\boldsymbol{x}) < p_t^{(i)} \right\} = \alpha \hat{P}_f^{i-1} \tag{20}$$

where $P\left\{ f_{\boldsymbol{X}}(\boldsymbol{x}) < p_t^{(i)} \right\}$ denotes the probability that the joint PDF of the random variables is smaller than $p_t^{(i)}$; $\hat{P}_f^{i-1}$ is the failure probability estimated from the established BSVR model in the $(i-1)$-th iteration of the learning process; α is the coefficient used to control the size of the sampling region and is taken as 0.1 in this study.

In each iteration, the threshold value $p_t^{(i)}$ can be obtained as the $(\alpha \hat{P}_f^{i-1})$-th percentile of the variable $\mathcal{F} = f_{\boldsymbol{X}}(\boldsymbol{x})$ by means of MCS. Once the sampling region as expressed in Eq. (19) is defined, the candidate samples for learning are generated in this region, thus those with small probability density will not be selected. In this way, the samples with negligible effects on the failure probability estimation will be filtered out, which can greatly enhance the efficiency of the learning algorithm. To facilitate a visual understanding of the idea underlying the SRS, two illustrative examples are given in Fig. 3, where $p_t^{(i)}$ is assumed to be 0.1 and $\alpha = 0.2$. It is noted that the MCS population consists of the samples being filtered out by SRS (blue points) and the remaining ones in the inner region (cyan points). In the learning process, only the cyan points will be used as the candidate points to select the next best sample.

3.2. Error-based stopping criterion using BCE

Besides the SRS as described in the previous section, choosing the appropriate stopping criterion can also improve the efficiency of the adaptive algorithm. One of the most widely used stopping criteria is derived by setting a threshold value for the learning function, as those presented in [25,26,30]. However, they are usually inadequate for the learning algorithm due to a lack of direct correspondence to the error of failure probability estimation, which is the parameter of particular interest. This limitation may lead to inaccurate failure probability estimation or results in a high computational burden because of unnecessary functional calls. To effectively address this issue, the error-based stopping criterion (ESC) expressed in terms of the upper bound of the estimation error is proposed in [32,33]. In this approach, the relative error ε_r of the predicted failure probability $\widehat{P}_f$ with respect to the reference result by MCS P_f^{MCS} is defined:

$$\varepsilon_r = \left| \frac{P_f^{\mathrm{MCS}} - \widehat{P}_f}{P_f^{\mathrm{MCS}}} \right| = \left| \frac{\frac{N_f}{N_{\mathrm{MCS}}} - \frac{\widehat{N}_f}{N_{\mathrm{MCS}}}}{\frac{N_f}{N_{\mathrm{MCS}}}} \right| = \left| \frac{\widehat{N}_f}{N_f} - 1 \right| \tag{21}$$

where N_{MCS} is the sample size of MCS, N_f is the number of failure samples evaluated from the true performance function, and $\widehat{N}_f$ denotes the number of failure samples determined by the surrogate model (e.g. BSVR). Let the true failure region and safe region in the random space Ω respectively be denoted as Ω_f and Ω_s, whereas those predicted by the surrogate are represented as $\hat{\Omega}_f$ and $\hat{\Omega}_s$. Then, the failure sample size N_f in Eq. (21) can be calculated as:

$$N_f = \widehat{N}_f + \widehat{N}_{sf} - \widehat{N}_{fs} \tag{22}$$

where $\widehat{N}_{sf}$ is the number of MCS samples in Ω_f while falling into $\hat{\Omega}_s$ predicted by the surrogate model, and $\widehat{N}_{fs}$ is the number of MCS samples in Ω_s while falling into $\hat{\Omega}_f$ in the prediction. Since the established surrogate model itself is a Gaussian random process, thus the $\widehat{N}_{sf}$ and $\widehat{N}_{fs}$ being predicted also follow some probabilistic distribution. In this regard, a confidence interval can be assigned to the failure sample size N_f:

$$N_f \in \left[\widehat{N}_f - \widehat{N}_{fs}^u, \quad \widehat{N}_f + \widehat{N}_{sf}^u \right] \tag{23}$$

where $\widehat{N}_{fs}^u$ and $\widehat{N}_{sf}^u$ are the upper bounds of the confidence interval of $\widehat{N}_{fs}$ and $\widehat{N}_{sf}$. Accordingly, the maximum relative error of the failure probability estimation can be expressed as:

$$\epsilon_r \leq \max \left(\left| \frac{\widehat{N}_f}{\widehat{N}_f - \widehat{N}_{fs}^u} - 1 \right|, \left| \frac{\widehat{N}_f}{\widehat{N}_f + \widehat{N}_{sf}^u} - 1 \right| \right) = \hat{\epsilon}_{\max} \tag{24}$$

Assuming that the sample size in $\hat{\Omega}_f$ and $\hat{\Omega}_s$ are sufficiently large, $\widehat{N}_{fs}^u$ and $\widehat{N}_{sf}^u$ are respectively determined as the upper confidence interval of a Poisson distribution and a normal distribution in [32,33]. However, this assumption may not be valid since the number of uncertain points decreases with the convergence of the learning process. Thus, an improved version of ESC using the bootstrap confidence estimation (BCE) has recently been developed in [34]. In the BCE-based ESC, only the highly uncertain samples near the LSS are considered instead of the whole population, in that the estimation error of failure probability is mainly contributed by these samples. Once the highly uncertain samples are defined, the upper bound values $\widehat{N}_{sf}^u$ and $\widehat{N}_{fs}^u$ can be calculated through the bootstrap resampling method, and the BCE-based ESC is formulated as:

$$\epsilon_r \leq \max \left(\left| \frac{\widehat{N}_f}{\widehat{N}_f - \widehat{N}_{fs}^u} - 1 \right|, \left| \frac{\widehat{N}_f}{\widehat{N}_f + \widehat{N}_{sf}^u} - 1 \right| \right) = \hat{\epsilon}_{\max} \leq \epsilon_{tol} \tag{25}$$

where ϵ_{tol} is a predefined threshold for the relative estimation error.

It is referred to [32–34] and references therein for more information about the ESC and BCE-based ESC, both of which are originally developed for Kriging-based approaches. In this study, only the BCE-based ESC will be used to develop the hybrid convergence criterion and further adapt to the ABSVR proposed in this paper.

4. The proposed new learning function

In structural reliability analysis, the evaluation of failure probability is essentially a classification problem whose estimation error is mainly contributed by samples reside around the LSS, i.e. $G(\boldsymbol{x}) = 0$, especially in regions with high prediction variance $\widehat{\sigma}^2_{\hat{g}}(\boldsymbol{x})$ and large probability density $f_X(\boldsymbol{x})$. In this regard, learning functions capable of identifying sample points with these desirable features are of particular interest to ensure the overall performance of the adaptive algorithm. Therefore, the learning process of an adaptive algorithm can equivalently be formulated as the following optimization problem to search for the most informative sample $\boldsymbol{x}^*$:

$$\begin{array}{ll} \text{find} & \boldsymbol{x}^* \\ \max & \widehat{\sigma}_{\hat{g}}(\boldsymbol{x})\rho(\boldsymbol{x})d_{\min}(\boldsymbol{x}) \\ \text{s.t.} & \left|\widehat{\mu}_{\hat{g}}(\boldsymbol{x})\right| = 0 \end{array} \tag{26}$$

where $\widehat{\mu}_{\hat{g}}(\boldsymbol{x})$ and $\widehat{\sigma}^2_{\hat{g}}(\boldsymbol{x})$ are respectively the prediction mean and variance of the surrogate model, e.g. Eqs. (15)–(18) for the two BSVR models; $d_{\min}(\boldsymbol{x})$ is the minimum distance of point $\boldsymbol{x}$ to those in the current DoE; $\rho(\boldsymbol{x})$ represents the value of joint PDF $f_X(\boldsymbol{x})$ evaluated at $\boldsymbol{x}$. According to the distribution information of random variables, $\rho(\boldsymbol{x})$ can be calculated in different ways, that is,

$$\rho(\boldsymbol{x}) = \begin{cases} f_X(\boldsymbol{x}) & \text{with known joint PDF} \\ \prod_i^n f_i(x_i) & \text{with uncorrelated random variables} \\ c\left(F_1\left(x_1\right), F_2\left(x_2\right), \ldots, F_n\left(x_n\right)\right) \prod_i^n f_i(x_i) & \text{with correlated random variables} \end{cases} \tag{27}$$

where $f_i(\boldsymbol{x})$ and $F_1\left(x_1\right)$ are the marginal PDF and the corresponding cumulative distribution function (CDF) of x_i, with x_i being the ith element of random vector $\boldsymbol{x}$; $c(\cdot)$ is the copula density function.

The objective function in Eq. (26) is formulated to find the representative samples that contribute to the improvement of the surrogate model for structural reliability analysis, and the equality constraint $\left|\widehat{\mu}_{\hat{g}}(\boldsymbol{x})\right| = 0$ ensures that the optimal solutions are in the vicinity of the LSS. In other words, the informative samples for model updating can be obtained by solving the constrained optimization problem expressed in Eq. (26). This, however, would introduce additional optimization algorithms into the learning process and complicate the adaptive algorithm, making the approach less user-friendly. To bypass this limitation, the constraint optimization problem is equivalently formulated as a sampling-based learning function for sample selection. Specifically, following the idea of the penalty function method, the proposed learning function utilizes a simple yet effective way to guide the search toward critical points near the LSS with a large probability density. Besides, a distance constraint term is introduced into the learning function to better control the density of samples in the DoE. Moreover, the inclusion of prediction variance in the learning function enables the efficient exploration of the regions with large uncertainty. The formulation of the proposed learning function is elucidated in the following subsections.

4.1. Identification of samples near the LSS in critical regions

In order to identify the new sample point $\boldsymbol{x}_{\text{new}}$ located in the vicinity of the LSS, a simple yet effective way is to transform the equality constraint $\left|\widehat{\mu}_{\hat{g}}(\boldsymbol{x})\right| = 0$ into an approximate unconstrained optimization problem by introducing a penalty term γ to the function. One possible formulation is given as follows:

$$\boldsymbol{x}_{\text{new}} = \underset{\boldsymbol{x}\in\boldsymbol{S}_C}{\arg\min} \left\{ 1 + \exp\left(\frac{\gamma \left|\widehat{\mu}_{\hat{g}}(\boldsymbol{x})\right|}{\widehat{\mu}_{\max}} \right) \right\} \tag{28}$$

where $\boldsymbol{S}_C$ is the candidate sampling pool; the introduction of the positive penalty term γ enables the penalty effect to work; the $\sigma_{\max} = \max(\left|\widehat{\mu}_{\hat{g}}(\boldsymbol{x})\right|)$ returns the maximum value of the absolute predictions at $\boldsymbol{S}_C$, which is introduced to reduce the magnitude effect to improve the flexibility of the algorithm. In this formula, the objective function tends to be minimized when $\left|\widehat{\mu}_{\hat{g}}(\boldsymbol{x})\right| = 0$, i.e. for points located on the LSS, while it becomes larger for points deviating farther from the LSS. Therefore, the points in the vicinity of LSS can be effectively identified from the candidate samples $\boldsymbol{S}_C$.

To ensure that the sample points are selected in the critical regions, i.e. regions with relatively large prediction uncertainty and probability density, the function in Eq. (28) is reformulated by adding the effects of BSVR prediction

variance $\widehat{\sigma}^2_{\hat{g}}(\boldsymbol{x})$ and joint PDF $f_{\mathbf{X}}(\boldsymbol{x})$ into the formulation, that is,

$$\boldsymbol{x}_{\text{new}} = \arg\min_{\boldsymbol{x}\in\boldsymbol{S}_C} \left\{ \frac{1+\exp\left(\frac{\gamma\left|\mu_{\hat{g}}(\boldsymbol{x})\right|}{\mu_{\max}}\right)}{10^{-8}+\frac{\sigma_{\hat{g}}(\boldsymbol{x})}{\sigma_{\max}}\cdot\frac{\rho(\boldsymbol{x})}{\rho_{\max}}} \right\} \tag{29}$$

where $\sigma_{\max}=\max(\widehat{\sigma}_{\hat{g}}(\boldsymbol{x}))$ is the maximum value of the standard deviation of BSVR model evaluated at $\boldsymbol{S}_C$; $\rho(\boldsymbol{x})$ is given in Eq. (27), and $\rho_{\max}=\max(\rho(\boldsymbol{x}))$. The very small value is introduced to avoid the denominator being zero; other smaller values can also be used as the learning function is insensitive to the value used. Learning through this function enables the new sample points close to the LSS with large probability density and prediction variance to be identified, which is expected to largely enhance the performance of BSVR-based reliability analysis.

4.2. A distance-based constraint

The learning process is highly likely to introduce points being close the existing ones when the learning function is formulated to focus only on points near the LSS in critical regions. These points contain little extra information for the refinement of the surrogate model, but may dramatically increase the computational burden. To address this issue, a distance constraint is integrated into the learning function developed in the previous subsection to avoid the clustering of sample points and thus improve the uniformity of the DoE.

The Euclidean distance is employed here to measure the distance between two points. Given a point $\boldsymbol{x}_C^i$ in the candidate set $\boldsymbol{S}_C$ (with a sample size of N_C) and a point $\boldsymbol{x}_D^j$ in the DoE $\boldsymbol{S}_D$ (with a sample size of N_D), the minimum distance of each sample point in $\boldsymbol{S}_C$ to those in $\boldsymbol{S}_D$ is calculated as:

$$d_{\min}(\boldsymbol{x}_C^i)=\min\left\{\sqrt{\left(\boldsymbol{x}_C^i-\boldsymbol{x}_D^j\right)^{\mathrm{T}}\left(\boldsymbol{x}_C^i-\boldsymbol{x}_D^j\right)}\right\}, i=1,2,\ldots,N_C;\ j=1,2,\ldots,N_D \tag{30}$$

with $\boldsymbol{d}_{\min}=\left\{d_{\min}(\boldsymbol{x}_C^1), d_{\min}(\boldsymbol{x}_C^2),\ldots,d_{\min}(\boldsymbol{x}_C^{N_C})\right\}$ denoting the vector of the minimum distances. Then the critical sample points with large values of $\boldsymbol{d}_{\min}$ are preferred to be chosen as the new samples in the DoE. With the inclusion of distance constraint, the density of samples in the DoE can effectively be controlled and accordingly, the clustering of samples is avoided.

4.3. The new learning function

Integrating the distance-based constraint term (Eq. (30)) into the learning function as expressed in Eq. (29), a Sampling-based Learning Function (SLF) capable of identifying informative points that disperse as far as possible from the existing ones can be devised as:

$$\text{SLF}: \quad \boldsymbol{x}_{\text{new}} = \arg\min_{\boldsymbol{x}\in\boldsymbol{S}_C} \left\{ \frac{1+\exp\left(\frac{\gamma\left|\mu_{\hat{g}}(\boldsymbol{x})\right|}{\mu_{\max}}\right)}{10^{-8}+\frac{\widehat{\sigma}_{\hat{g}}(\boldsymbol{x})}{\sigma_{max}}\cdot\frac{\rho(\boldsymbol{x})}{\rho_{max}}\cdot d_{\min}(\boldsymbol{x})} \right\} \tag{31}$$

Unlike the well-known learning function U that cannot be used for points located exactly on the LSS, i.e. $|\widehat{\mu}(\boldsymbol{x})|=0$, the proposed learning function SLF still works for this particular case. To further improve the convergence speed of the learning process, the candidate samples $\boldsymbol{S}_C$ are generated using the Sobol sequences given its uniformity and space-filling property. It is noted that other low-discrepancy sequences can also be used for the same purpose.

5. A hybrid stopping criterion

The use of BCE-based stopping criterion (BCE-based ESC) as described in Section 3.2 can greatly enhance the computational efficiency with the upper bound of estimation error controlled at a specified level. However, there are cases that the accuracy of the failure probability estimation tends to be stabilized before the BCE-based ESC is satisfied, which implies that adding additional samples after this stage will not contribute much to the improvement

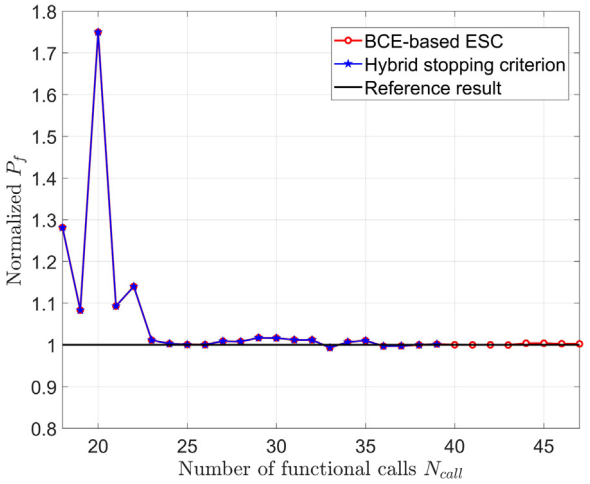

Fig. 4. Convergence of the failure probability using different stopping criteria.

of the surrogate model, but rather increase the computational burden of the algorithm. To alleviate the potentially high computational cost, a hybrid stopping criterion that can detect the stabilization stage of failure probability estimation during the learning process is developed in this section.

To effectively detect the stabilization stage of failure probability estimation, a feasible way is to define a criterion utilizing the reliability indices acquired in consecutive iterations. In this study, three consecutive estimations (when the iteration number $i \geq 5$) are employed for this purpose, that is:

$$\left|\frac{\widehat{\beta}_i - \widehat{\beta}_{i-1}}{\widehat{\beta}_{i-1}}\right| < \epsilon_{tol1}, \quad \left|\frac{\widehat{\beta}_{i-1} - \widehat{\beta}_{i-2}}{\widehat{\beta}_{i-2}}\right| < \epsilon_{tol1} \quad \text{and} \quad \left|\frac{\widehat{\beta}_{i-2} - \widehat{\beta}_{i-3}}{\widehat{\beta}_{i-3}}\right| < \epsilon_{tol1}, i \geq 5 \tag{32}$$

where $\widehat{\beta}_i$, $\widehat{\beta}_{i-1}$, $\widehat{\beta}_{i-2}$ and $\widehat{\beta}_{i-3}$ are the reliability indices (i.e. $\widehat{\beta} = -\Phi^{-1}\left(\widehat{P_f}\right)$, with $\Phi^{-1}(\cdot)$ denoting the inverse of standard normal CDF) estimated in the current, the $(i-1)$th, the $(i-2)$th and the $(i-3)$th iterations, respectively; and ϵ_{tol1} is the convergence threshold defined in the range of $[10^{-5}, 10^{-3}]$. However, directly apply Eq. (32) as a stopping criterion may lead to inaccurate failure probability estimation due to premature of the learning process. Therefore, the BCE-based stopping criterion is integrated with Eq. (32) to derive a new one, which is expressed as:

$$\begin{cases} \left|\frac{\widehat{\beta}_i - \widehat{\beta}_{i-1}}{\widehat{\beta}_{i-1}}\right| < \epsilon_{tol1}, \quad \left|\frac{\widehat{\beta}_{i-1} - \widehat{\beta}_{i-2}}{\widehat{\beta}_{i-2}}\right| < \epsilon_{tol1} \quad \text{and} \quad \left|\frac{\widehat{\beta}_{i-2} - \widehat{\beta}_{i-3}}{\widehat{\beta}_{i-3}}\right| < \epsilon_{tol1}, i \geq 5 \\ \max\left(\left|\frac{\widehat{N}_f}{\widehat{N}_f - \widehat{N}^u_{fs}} - 1\right|, \left|\frac{\widehat{N}_f}{\widehat{N}_f + \widehat{N}^u_{sf}} - 1\right|\right) = \hat{\epsilon}_{\max} \leq \epsilon_{tol2} \end{cases} \tag{33}$$

where the predefined threshold $\epsilon_{tol2} \in [0.005, 0.1]$ can generally lead to a trade-off between accuracy and efficiency.

Similarly, an additional stabilization detection term is added to the original BCE-based ESC (i.e. Eq. (25)), i.e.,

$$\begin{cases} \max\left(\left|\frac{\widehat{N}_f}{\widehat{N}_f - \widehat{N}^u_{fs}} - 1\right|, \left|\frac{\widehat{N}_f}{\widehat{N}_f + \widehat{N}^u_{sf}} - 1\right|\right) = \hat{\epsilon}_{\max} \leq \epsilon_{tol3} \\ \left|\frac{\widehat{\beta}_i - \widehat{\beta}_{i-1}}{\widehat{\beta}_{i-1}}\right| < \epsilon_{tol4}, i \geq 5 \end{cases} \tag{34}$$

where ϵ_{tol3} and ϵ_{tol4} are the given threshold values for the BCE-based ESC and the stabilization detection term, respectively. In this criterion, the BCE-based ESC will not be activated until the stability condition is fulfilled.

It is noteworthy that although Eq. (33) is similar to Eq. (34) in the form, they are defined for different purpose. Specifically, Eq. (33) is mainly defined to avoid unnecessary calls once the failure probability estimation is detected to have stabilized with a certain precision, whereas Eq. (34) is defined to control the estimation error and thus ensure the overall accuracy of the algorithm. To achieve this, the ϵ_{tol1} in Eq. (33) can be set to a smaller value than the ϵ_{tol4} in Eq. (34), e.g. $\epsilon_{tol1} = 10^{-4}$ and $\epsilon_{tol4} = 10^{-3}$; while the BCE-based ESC threshold ϵ_{tol2} in Eq. (33) can be set to a larger value than its counterpart defined in Eq. (34), e.g. $\epsilon_{tol2} = 0.1$ and $\epsilon_{tol3} = 0.01$.

Therefore, the proposed hybrid stopping criterion consists of two separate criteria as expressed in Eqs. (33) and (34), and the active learning process is terminated when any one of them is fulfilled. An example is shown in Fig. 4

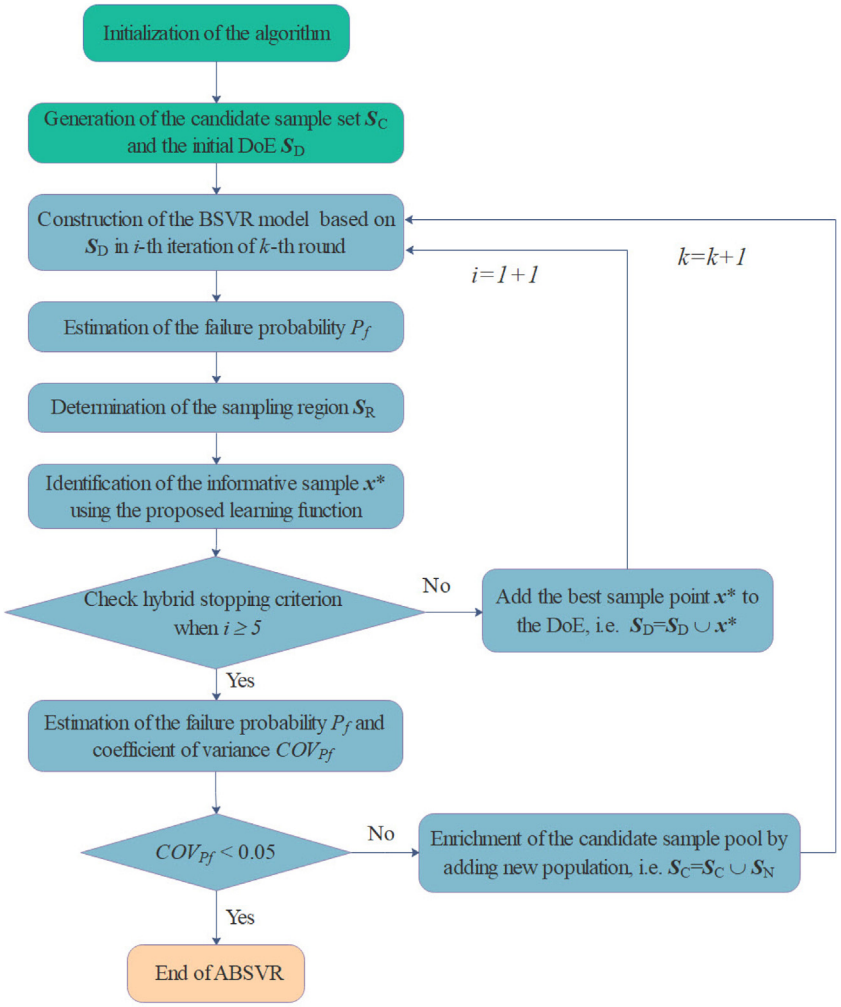

Fig. 5. Flowchart of the ABSVR.

to illustrate the potential gain of this hybrid stopping criterion as compared with the original BCE-based ESC. In this example, $\epsilon_{tol1} = 10^{-4}$, $\epsilon_{tol2} = 0.2$, $\epsilon_{tol3} = 0.02$ and $\epsilon_{tol4} = 10^{-2}$ for the hybrid criterion; $\epsilon_{tol} = 0.02$ for BCE-based ESC. It is seen that the failure probability has stabilized before the BCE-based ESC is fulfilled, and the proposed approach can detect this phenomenon and stop the algorithm with a reduced number of functional calls.

6. Implementation procedure of ABSVR

Combining the advanced schemes, the proposed learning function and the hybrid stopping criterion with the BSVR model, two Adaptive algorithms based on the BSVR (ABSVR) are proposed in this study, namely the one based on SLF (ABSVR1) and the one based on EISLF (ABSVR2). These two ABSVR methods start from a small initial DoE and iteratively refine the BSVR model by progressively enriching the DoE according to the proposed learning function. The learning process is repeated until the hybrid stopping criterion is met, then the failure probability can easily be estimated from the established BSVR model. Obviously, the only difference between ABSVR1 and ABSVR2 is the loss function used to construct the BSVR model. The flowchart of the ABSVR methods is depicted in Fig. 5 with 8 steps as summarized below:

- **Step 1**: Initialization of the algorithm. The parameters in ABSVR are initialized, including the sample size N_C in the candidate set $\boldsymbol{S}_C$, the sample size N_0 in the initial DoE, the positive penalty factor γ in the learning function (Eq. (31)), and the convergence thresholds $\epsilon_{toli}, i = 1, 2, 3, 4$ in Eqs. (33) and (34).
- **Step 2**: Generation of the candidate sample set $\boldsymbol{S}_C$ and initial DoE $\boldsymbol{S}_D$. To generate the Sobol sequence for $\boldsymbol{S}_C$, the UQLab [58] is employed in this study. Samples in the initial DoE are generated using Latin hypercube sampling (LHS) with a sample size of $N_0 = 15$.
- **Step 3**: Construction of the BSVR model. The generated DoE $\boldsymbol{S}_D$ is applied to build the BSVR model, based on which the prediction mean $\mu_{\widehat{g}}(\boldsymbol{x})$ and variance $\sigma^2_{\widehat{g}}(\boldsymbol{x})$ of the samples in $\boldsymbol{S}_C$ can be evaluated from Eqs. (15) and (16) for ABSVR1, and from Eqs. (17) and (18) for ABSVR2. To calibrate the BSVR model, the hyperparameters may be found using any general-purpose optimization algorithm by solving the optimization problems defined in Eq. (12) or Eq. (14). In the present study, the initial values of these parameters are defined as $\eta = 10^5, \epsilon = 10^{-5}$, and $\theta_k = 1, k = 1, 2, \ldots, n$. According to the study performed in [16], it is desirable to define high optimization bound for the regularization parameter η and low optimization bound for the insensitive tube width ϵ. Thus, relatively wide ranges are selected for these parameters, namely $\left[10, 10^{10}\right]$ for η, $\left[10^{-8}, 0.01\right]$ for ϵ, and $\left[10^{-5}, 10^5\right]$ for θ_k. The interior-point algorithm in Matlab is employed to solve the associated optimization problems.
- **Step 4**: Generation of the reduced sample set $\boldsymbol{S}_R$ through the sampling region scheme expressed in Eq. (20). The failure probability is evaluated according to Eq. (3) with the true model being replaced by the BSVR model, and the points in $\boldsymbol{S}_R$ are obtained by filtering out the sample points with rather small probability density in $\boldsymbol{S}_C$.
- **Step 5**: Selection of informative samples to enrich the DoE. In each iteration, the sample point $\boldsymbol{x}^*$ in $\boldsymbol{S}_R$ that minimize the learning function Eq. (31) is selected as the optimal one, whose model response is evaluated by calling the true performance function. Therefore, each time the DoE is enriched with the new sample point ($\boldsymbol{S}_D = \boldsymbol{S}_D \cup \boldsymbol{x}^*$) and $N_0 = N_0 + 1$. This learning process is repeated (i.e. iteration number $i = i + 1$) from Step 3 to Step 5 until one of the conditions in the hybrid stopping criterion is fulfilled.
- **Step 6**: Computation of the coefficient of variation. To ensure that the sample size in $\boldsymbol{S}_C$ is large enough to provide reliable failure probability estimation $\hat{P}_f$, the coefficient of variation below 5% is acceptable, that is,

$$Cov = \sqrt{\frac{1 - \widehat{P}_f}{N_C \widehat{P}_f}} < 0.05 \tag{35}$$

- **Step 7**: Enrichment of the population in $\boldsymbol{S}_C$. If the condition in Eq. (35) is not met, $\boldsymbol{S}_C$ is enriched with new sample population $\boldsymbol{S}_N$, and the learning algorithm goes back to Step 3 and carries on until all the stopping criteria are fulfilled; otherwise, proceed to Step 8.
- **Step 8**: End of ABSVR. If the stopping condition expressed in Eq. (35) is met, the whole learning algorithm is terminated and the failure probability is evaluated on the final BSVR model.

7. Numerical examples

In this section, the accuracy, efficiency, and robustness of the proposed method are investigated using six numerical examples. To show the robustness of the ABSVR, all results are obtained by averaging over 10 repeated runs of the algorithm, including the failure probability $\hat{P}_f$, the reliability index $\widehat{\beta}$, the total number of functional calls N_f and the relative error of failure probability $\epsilon_{\hat{P}_f}$. These results are compared with those of MCS and other existing methods whenever possible. In this paper, the relative error of failure probability $\epsilon_{\hat{P}_f}$ is calculated as:

$$\epsilon_{\hat{P}_f} = \frac{\left|\widehat{P}_f - \hat{P}_f^{MCS}\right|}{\hat{P}_f^{MCS}} \times 100\% \tag{36}$$

where $\hat{P}_f^{MCS}$ denotes the reference result provided by MCS, $\widehat{P}_f$ is the failure probability estimated from methods other than MCS, e.g. FORM, SORM, IS and AK-MCS+U. It is noted that the results of FORM, SORM and IS are calculated using the UQLab [59].

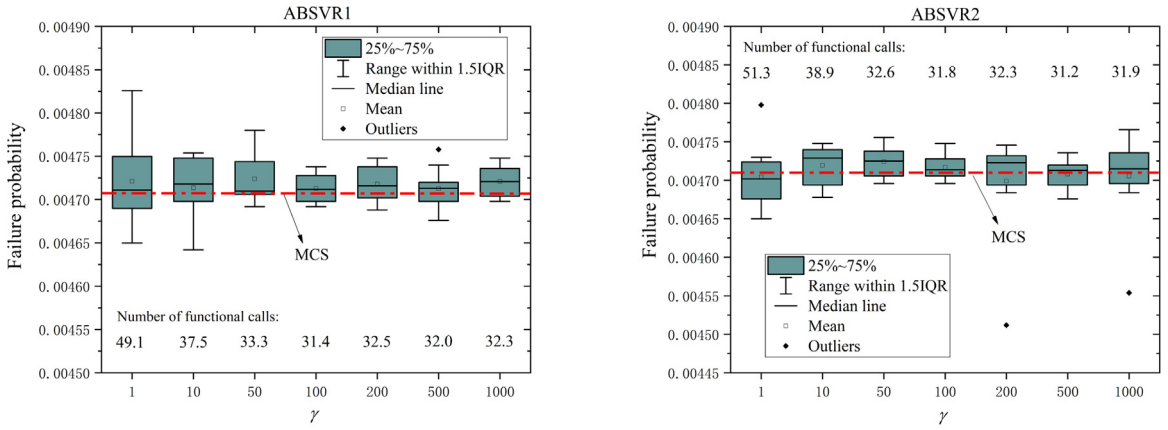

Fig. 6. Boxplots of the results for ABSVR using different values of γ: (a) The failure probability estimation; (b) The functional calls. (For interpretation of the references to color in this figure, please refer to the web version of this article.)

7.1. Example 1: A highly nonlinear problem

This example considers a 2D high nonlinearity problem with a single failure region, which has been previously been studied in [25,30,34]. The performance function of this problem is formulated as:

$$g(\boldsymbol{x}) = 1.2 - \frac{1}{20}\left(x_1^2 + 4\right)(x_2 - 1) + \sin\left(\frac{5}{2}x_1\right) \tag{37}$$

where x_1 and x_2 are two independent standard normal variables. In order to determine appropriate values of the parameters involved in the proposed algorithm, namely the positive penalty factor γ and the convergence thresholds $\epsilon_{toli}, i = 1, 2, 3, 4$, a comprehensive parametric study is carried out first before making comparisons with other methods.

7.1.1. Effects of the positive penalty factor γ

In this subsection, a parametric study is carried out to investigate the influence of the penalty factor γ on the performance of the proposed algorithm. The analysis results with the penalty factor γ varying from 1 to 1000 are given in Fig. 6, where the averaged number of calls to the performance function over 10 repeated runs are also included. It is observed from Fig. 6 that all the averaged results provided by ABSVR using different values of γ are in close agreement with the MCS result (red dotted line). However, a large variation of failure probability is observed when $\gamma < 100$, and the robustness of the algorithm is enhanced when $\gamma \geq 100$. Moreover, a large number of functional calls is required for the algorithm with a small value of γ, yet the efficiency of the algorithm is relatively insensitive to the value of γ when $\gamma \geq 100$. This is because the points with large values of $\left|\widehat{\mu}_{\hat{g}}(\boldsymbol{x})\right|$ (for points deviating from the LSS) cannot be effectively penalized when γ is taken as a small value, say $\gamma = 1$, thus the samples on the limit state surface can hardly be identified. An example is illustrated in Fig. 7, where the converged ABSVR2 models with $\gamma = 1$ and $\gamma = 100$ are depicted. It is observed that the new samples selected by the learning function with $\gamma = 1$ deviate largely from the LSS, while those selected by the one with $\gamma = 100$ are all in the vicinity of the LSS. Therefore, the penalty factor γ has certain effects on the performance of ABSVR, and $\gamma \geq 100$ is generally preferred to reach a good trade-off between accuracy and efficiency. In this study, the learning function $\gamma = 100$ is used to demonstrate the performance of ABSVR for structural reliability analysis.

7.1.2. Effects of the threshold parameters

Basically, a total of four threshold parameters (i.e. $\epsilon_{toli}, i = 1, 2, 3, 4$) are involved in the proposed hybrid stopping criterion. Earlier experience suggests that the proposed algorithm can reach a good trade-off by setting

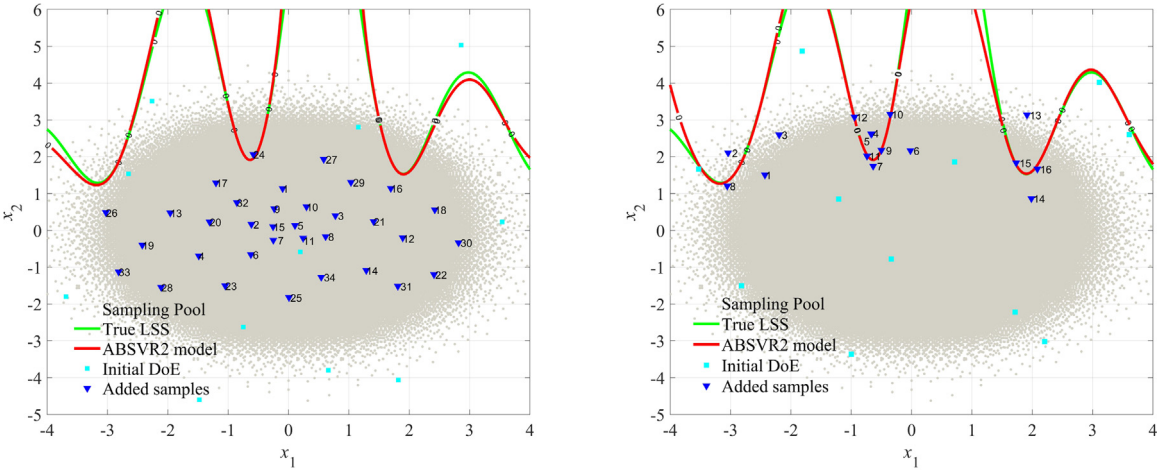

Fig. 7. The converged ABSVR2 model: (a) $\gamma = 1$; (b) $\gamma = 100$. (For interpretation of the references to color in this figure, please refer to the web version of this article.)

$\epsilon_{tol4} = 10^{-2}$, and the added value of smaller ϵ_{tol4} is negligible, yet more functional calls will be consumed. Therefore, a parametric study of the other three threshold parameters (e.g. ϵ_{tol1}, ϵ_{tol2} and ϵ_{tol3}) is conducted, with the value of ϵ_{tol4} being fixed at 10^{-2}. The averaged failure probabilities over 10 repeated runs of ABSVR2 with different combinations of threshold values are shown in Fig. 8. It is observed that the accuracy and efficiency of the algorithm are mainly affected by ϵ_{tol3}, whereas the influence of ϵ_{tol1} and ϵ_{tol2} is less obvious. The reason is that the stabilization detection criterion in Eq. (33) is introduced to identify the stabilization stage and is activated only when the learning process is found to have stabilized (which is detected by ϵ_{tol1}) with certain accuracy (which is controlled by ϵ_{tol2}). Therefore, the learning process of the algorithm is terminated by Eq. (34) most of the time, e.g. 8 out of 10 different runs. Specifically, less functional calls are required for a larger value of ϵ_{tol3} (less accurate of the analysis result though), and the algorithm is more robust when $\epsilon_{tol3} \leq 0.02$; the erroneous result might be obtained when the combination of $\epsilon_{tol1} = 10^{-3}$ and $\epsilon_{tol2} = 0.3$ is selected for the stopping criterion because of the premature of the algorithm. Therefore, to ensure the overall performance of the ABSVR, $\epsilon_{tol1} = 10^{-4}$, $\epsilon_{tol2} = 0.1$, $\epsilon_{tol3} = 0.01$ and $\epsilon_{tol4} = 10^{-2}$ is adopted as the default setting, if not specified otherwise.

7.1.3. Comparison with other methods

The results of these two ABSVRs are compared with those provided by MCS, FORM, SORM, AK-MCS+U\AK-MCS+EFF [26], REIF\REIF2 [30] and AK-SDMCS [37], as summarized in Table 1. The reference result of this example is obtained using MCS with 1×10^6 samples, i.e. $\widehat{P}_f = 4.71 \times 10^{-3}$ with a coefficient of variation $\delta_{P_f} = 1.45\%$, which is directly taken from [30]. It is seen from Table 1 that FORM is unable to deliver accurate failure probability prediction for this case, in that the nonlinear failure features cannot be captured by the first-order Taylor expansion, hence leading to an estimation error $\epsilon_{\hat{P}_f} > 100\%$. Although the accuracy of FORM can significantly be improved by SORM, the relative error is still unacceptably high, i.e. 22.06%, let alone more functional calls are required. On the contrary, all the investigated adaptive algorithms, including the Kriging-based approaches and the proposed BSVR-based ones, are capable of providing accurate failure probability prediction with high efficiency, i.e. the relative error $\epsilon_{\hat{P}_f}$ is less than 1% with no more than 50 functional calls. Among these adaptive algorithms, the two proposed ABSVRs exhibit better overall performance, indicating the effectiveness of ABSVRs for a problem with high nonlinearity.

To further illustrate the superior performance of ABSVRs, the converged BSVR models and the convergence history of failure probabilities corresponding to a single run of ABSVR1 and ABSVR2 are plotted in Figs. 9 and 10, respectively. It is observed from Figs. 9(a) and 10(a) that all the newly selected sample points (blue triangles with sequence number) are located in the vicinity of LSS and spread uniformly, resulting in an excellent match of the established BSVR models with the true one in critical regions. Accordingly, fast convergence of the failure

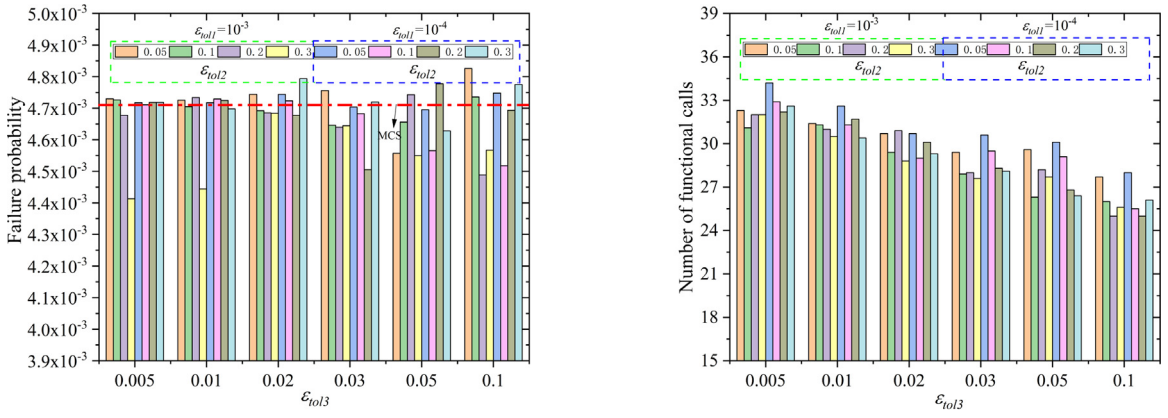

(a) (b)

Fig. 8. Reliability analysis results of ABSVR2 with different threshold values in the hybrid stopping criterion: (a) The failure probabilities; (b) The number of functional calls.

Table 1
Reliability analysis results for Example 1 using different methods.

Methods	$\hat{P}_f$	$\widehat{\beta}$	N_f	$\epsilon_{\hat{P}_f}$ (%)
MCS	4.710×10^{-3}	2.5964	1×10^6	–
FORM	2.563×10^{-2}	1.9492	779	>100
SORM	3.671×10^{-3}	2.6809	791	22.06
REIF	4.720×10^{-3}	2.5957	42.3	0.23
REIF2	4.710×10^{-3}	2.5964	35.6	0.03
AK-MCS+U	4.689×10^{-3}	2.5980	49.4	0.45
AK-MCS+EFF	4.742×10^{-3}	2.5941	49.8	0.67
AK-SDMCS	4.667×10^{-3}	2.5997	41.3	0.92
ABSVR1	4.723×10^{-3}	2.5953	32.6	0.28
ABSVR2	4.719×10^{-3}	2.5962	31.5	0.19

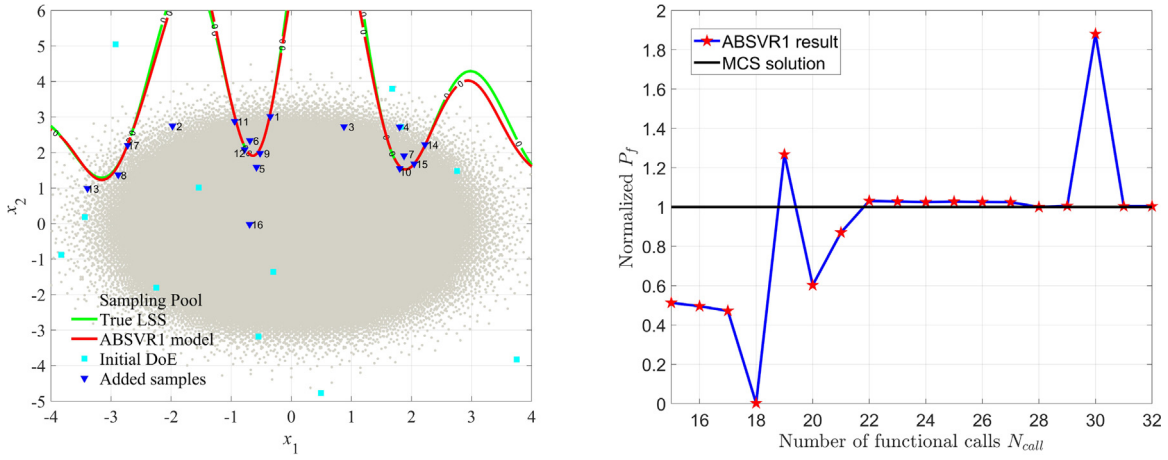

(a) (b)

Fig. 9. Results for a single run of ABSVR1: (a) The converged BSVR model; (b) The convergence history of failure probability. (For interpretation of the references to color in this figure, please refer to the web version of this article.)

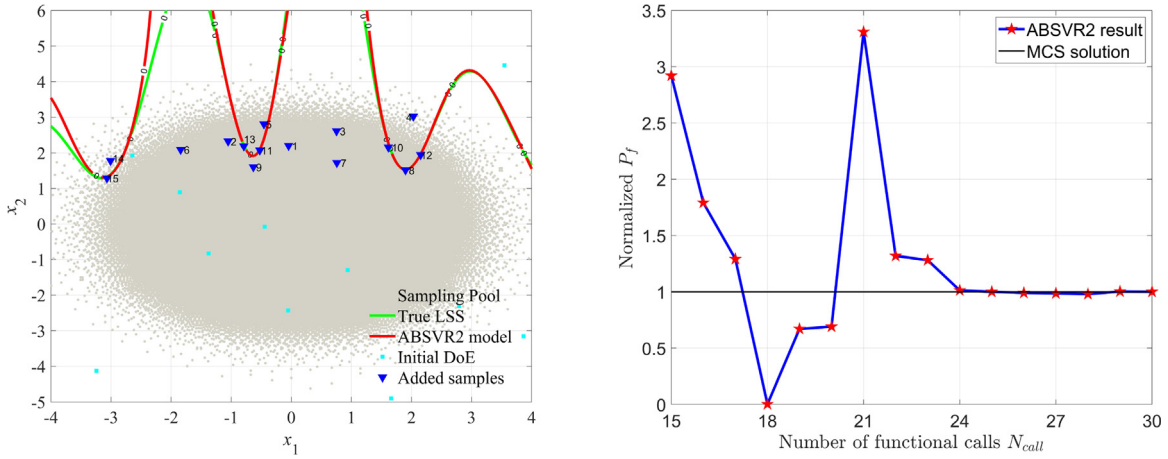

(a) (b)

Fig. 10. Results for a single run of ABSVR2: (a) The converged BSVR model; (b) The convergence history of failure probability. (For interpretation of the references to color in this figure, please refer to the web version of this article.)

probability estimation is observed after fluctuating significantly in the few iterations, as shown in Figs. 9(b) and 10(b). These results demonstrate the effectiveness of the proposed learning function (i.e. SLF) for identifying informative samples. Moreover, it is noteworthy that the LSS being poorly approximated at locations with low probability densities does not necessarily result in a poor estimation of the failure probability, in that the regions with extremely weak probability densities have little contribution to the prediction result.

7.2. Example 2: A series system with four branches

The second example is a series system with four branches, whose performance function is given as follows [26,34]:

$$g(\boldsymbol{x}) = \min \left\{ \begin{array}{c} 3 + 0.1\,(x_1 - x_2)^2 - \frac{x_1+x_2}{\sqrt{2}} \\ 3 + 0.1\,(x_1 - x_2)^2 + \frac{x_1+x_2}{\sqrt{2}} \\ (x_1 - x_2) + \frac{7}{\sqrt{2}} \\ (x_2 - x_1) + \frac{7}{\sqrt{2}} \end{array} \right\} \tag{38}$$

where x_1 and x_2 are two standard normal random variables. The failure probability of this series system is calculated by the proposed ABSVRs and compared with various other methods, among which the MCS (with a sample size of 1×10^7) reported in [34] is used as the reference result, i.e. $\hat{P}_f = 2.221 \times 10^{-3}$ with a coefficient of variation smaller than $\delta_{P_f} = 1\%$. The results of AK-MCS+U and AK-MCS+EFF [26], Neural Network-based Importance Sampling (NNIS) [60], Neural Network-based Directional Simulation (NNDS) [60], Active Deep Neural Network method (ADNN) [24] and ESC+RLCB [34] from the corresponding references are also listed for comparison purpose, as shown in Table 2.

One can see from Table 2 that the results calculated from traditional one-shot sampling schemes, namely the NNIS and the NNDS exhibit large estimation errors, i.e. respectively with a relative error of 30.57% and 54.98%, even at the expense of larger computational effort. In contrast to these non-adaptive algorithms, the estimation carried out by adaptive algorithms can generally achieve a good trade-off between accuracy and efficiency. Specifically, the proposed ABSVR1 and ABSVR2 provide comparable results (slightly better) on failure probability using fewer model evaluations as compared with AK-MCS+U and AK-MCS+EFF, and reach higher precision than ADNN with less functional calls.

The converged BSVR models and the convergence history of failure probability corresponding to a single run of ABSVR1 and ABSVR2 are depicted in Fig. 11 and Fig. 12, respectively. As can be seen from Figs. 11(a) and 12(a) that the initial sampling points (cyan square points) in DoE are spread over the random space, whereas the

Table 2
Reliability analysis results for Example 2 using different methods.

Methods	$\hat{P}_f$	$\widehat{\beta}$	N_f	$\epsilon_{\hat{P}_f}$ (%)
MCS	2.221×10^{-3}	2.845	1×10^7	–
AK-MCS+U	2.233×10^{-3}	2.843	96	0.54
AK-MCS+EFF	2.232×10^{-3}	2.843	101	0.50
NNIS	2.900×10^{-3}	2.760	125	30.57
NNDS	1.000×10^{-3}	3.050	67	54.98
ADNN	2.192×10^{-3}	2.849	70	1.31
ESC+RLCB	2.265×10^{-3}	2.839	43.8	1.98
ABSVR1	2.214×10^{-3}	2.846	39.6	0.34
ABSVR2	2.222×10^{-3}	2.845	42.8	0.04

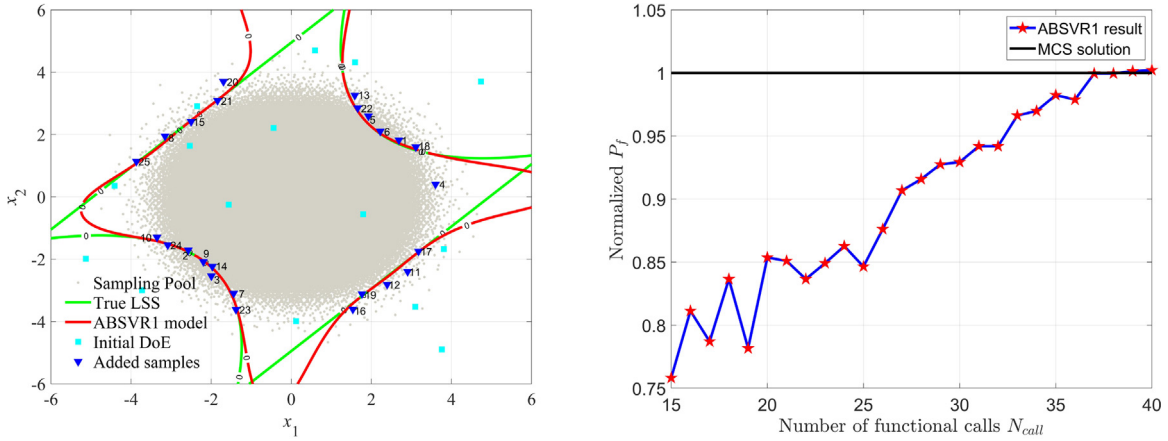

Fig. 11. Results from a single run of ABSVR1: (a) The converged BSVR model; (b) The convergence history of failure probability. (For interpretation of the references to color in this figure, please refer to the web version of this article.)

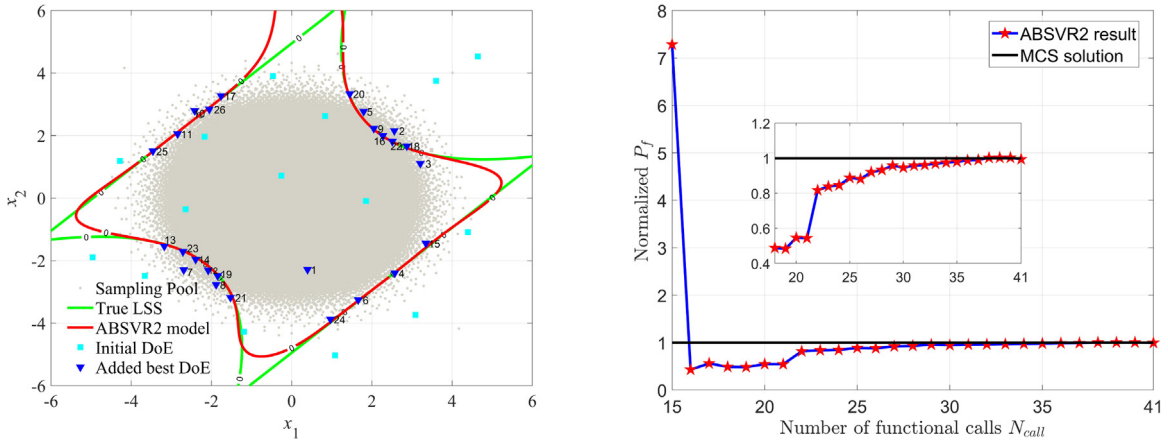

Fig. 12. Results from a single run of ABSVR2: (a) The converged BSVR model; (b) The convergence history of failure probability. (For interpretation of the references to color in this figure, please refer to the web version of this article.)

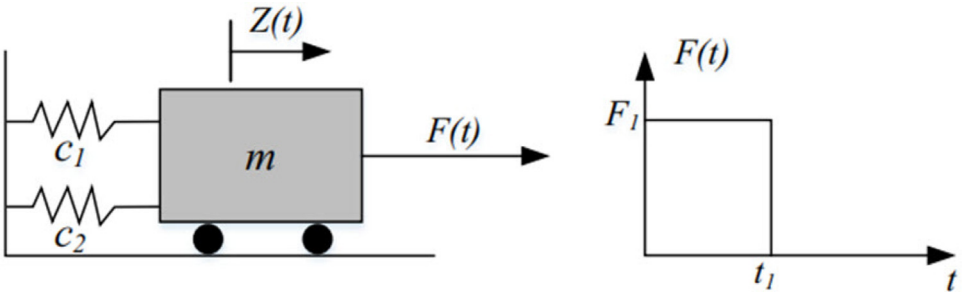

Fig. 13. Nonlinear oscillator subjected to a rectangular load pulse.

Table 3
Statistical information of the random variables.

Random variable	Distribution	Mean	Standard deviation
m	Normal	1	0.05
c_1	Normal	1	0.1
c_2	Normal	0.1	0.01
r	Normal	0.5	0.05
t_1	Normal	1	0.2
F_1 (Case 1)	Normal	1	0.2
F_1 (Case 2)	Normal	0.45	0.075

newly enriched points (blue triangles with sequence number) are uniformly distributed along the LSS in the regions of interest. This implies that the proposed SLF is capable of guiding the search toward a converged BSVR model that perfectly matches with the true one in the critical regions, leading to the fast convergence of both ABSVR1 and ABSVR2 for failure probability estimation, as shown in Figs. 11(b) and 12(b). Similar to Example 1, the poor fitting property of the ABSVR model in regions with rather low probability density (i.e. the four corners) will not mitigate the prediction accuracy since their contribution to failure probability is negligible.

7.3. Example 3: Dynamic response of a nonlinear oscillator

This example considers a nonlinear oscillator subjected to a rectangular load pulse, as shown in Fig. 13. It is an undamped single degree of freedom system, which has been investigated in numerous studies [17,26,61,62]. The performance function of this nonlinear system is expressed as:

$$g\left(c_1, c_2, m, r, t_1, F_1\right) = 3r - \left|\frac{2F_1}{m\omega_0^2}\sin\left(\frac{\omega_0 t_1}{2}\right)\right| \tag{39}$$

where $\omega_0 = \sqrt{\left(c_1 + c_2\right)/m}$, and the distribution parameters of these random variables are listed in Table 3.

7.3.1. Reliability analysis for case 1

In this case, the reference result is calculated from MCS with a sample size of 1×10^7 and the corresponding failure probability is 2.859×10^{-2}. The results calculated from FORM and SORM, and those by adaptive Kriging approaches, namely the AK-MCS\AK-MCSi\AK-MSS [63], and the AK-SS\AWL-MCS [62] directly taken from the corresponding references are also used for comparison purpose, as summarized in Table 4 along with the results provided by the proposed ABSVRs.

One can see from Table 4 that the failure probability estimated by FORM exhibits the largest error (i.e. $\epsilon_{\hat{P}_f} = 8.71\%$) among the investigated methods, albeit its high efficiency for this particular case. The accuracy of FORM can be improved by SORM, but at the expense of substantially higher computational effort than FORM, i.e. the total number of functional calls N_f increased from 48 to 128. Although AK-MCS and AK-SS both exhibit high precision, i.e. respectively with a relative error $\epsilon_{\hat{P}_f} = 0.24\%$ and $\epsilon_{\hat{P}_f} = 0.91\%$, the required number of functional calls is

Table 4
Reliability analysis results for Example 3 — Case 1 using different methods.

Methods	$\hat{P}_f$	$\widehat{\beta}$	N_f	$\epsilon_{\hat{P}_f}$ (%)
MCS	2.859×10^{-2}	1.902	1×10^7	–
FORM	3.108×10^{-2}	1.865	48	8.71
SORM	2.900×10^{-2}	1.896	128	1.43
AK-MCS	2.852×10^{-2}	1.903	530	0.24
AK-SS	2.833×10^{-2}	1.906	410	0.91
AK-MCSi	2.830×10^{-2}	1.906	85	1.01
AK-MSS	2.870×10^{-2}	1.900	86	0.38
AWL-MCS	2.826×10^{-2}	1.907	65	1.15
ABSVR1	2.855×10^{-2}	1.903	46.8	0.15
ABSVR2	2.871×10^{-2}	1.900	45.4	0.41

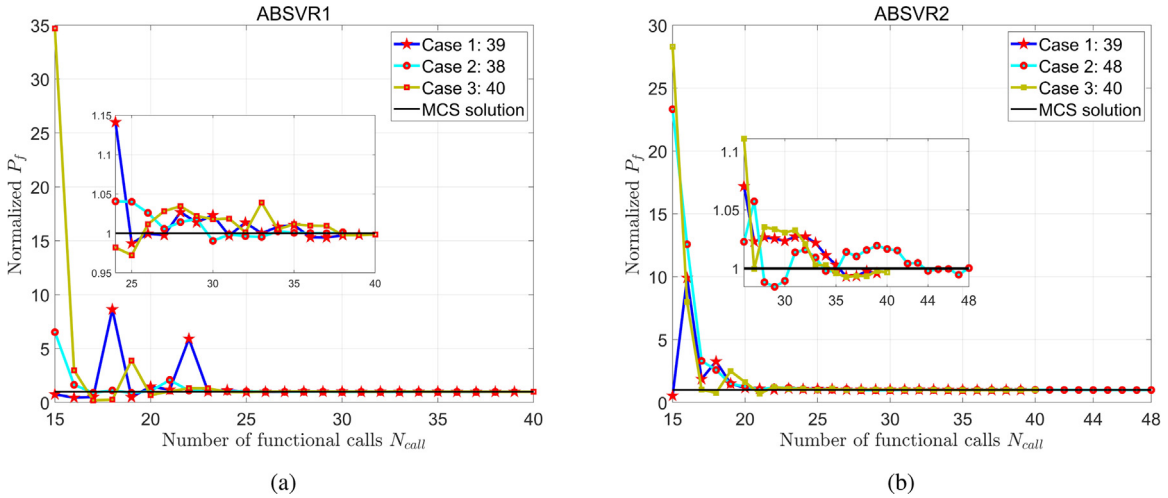

(a) (b)

Fig. 14. The convergence history of failure probability: (a) The results of ABSVR1; (b) The results of ABSVR2. (For interpretation of the references to color in this figure, please refer to the web version of this article.)

prohibitively high compared with other adaptive algorithms. On the contrary, the other three adaptive Kriging-based approaches, namely the AK-MCSi, the AK-MSS and the AWL-MCS are capable of providing a balanced performance for this case. Remarkably, the proposed ABSVR1 and ABSVR2 show excellent performance in terms of accuracy and efficiency, i.e. with a relative error less than 0.5% using less than 50 functional calls, indicating the capability of ABSVRs to reach a balanced performance for structural reliability analysis of this dynamic system. The convergence history of failure probability by three independent runs of ABSVRs are depicted in Fig. 14, where the estimation results are seen to have quickly converged to the reference solution for both ABSVR1 and ABSVR2 after fluctuated significantly in the first 8 iterations.

7.3.2. Reliability analysis for case 2

For problems with extremely low failure probabilities, the MCS-based adaptive algorithm is not efficient since the required number of candidate samples is prohibitively high. To address this issue, the adaptive algorithms can be combined with advanced simulation methods such as importance sampling (IS) [35,64] and subset simulation (SS) [63] to further improve computational efficiency. For illustrative purposes, the proposed algorithm is integrated with the IS presented in [35] to investigate its applicability to rare failure events. In this approach, the center of the importance sampling density is the most probable point (does not have to be very accurate) being found by FORM in a few iterations (3 iterations in this case), and the samples generated from the importance density are used as the candidate samples in the learning process, which is quite different from the MCS-based approaches.

The reference result obtained by MCS is 1.55×10^{-8} with a coefficient of variation equal to 2.68%, and the results of FORM and SORM are calculated using the UQLab [59]. The results of the proposed algorithm along with various

Table 5
Reliability analysis results for Example 3 — Case 2 using different methods.

Methods	$\hat{P}_f$	$\widehat{\beta}$	N_f	$\epsilon_{\hat{P}_f}$ (%)
MCS*	1.55×10^{-8}	5.536	9×10^{10}	–
FORM	1.56×10^{-8}	5.535	96	0.65
SORM	1.52×10^{-8}	5.540	176	1.94
AK-IS*	1.53×10^{-8}	5.538	67	1.29
AK-MCSi*	1.44×10^{-8}	5.549	77	7.10
AK-ARBIS*	1.56×10^{-8}	5.535	76	0.65
ABSVR1-IS	1.50×10^{-8}	5.542	38.6	3.27
ABSVR2-IS	1.53×10^{-8}	5.538	43.9	1.29

Note: * Results reproduced from [64].

Table 6
Reliability analysis results for Example 4 using different methods.

Methods	$\hat{P}_f$	$\widehat{\beta}$	N_f	$\epsilon_{\hat{P}_f}$ (%)
MCS	1.978×10^{-3}	2.882	1×10^{6}	–
FORM	2.152×10^{-4}	3.521	168	89.12
SORM	2.494×10^{-3}	2.808	3410	26.09
AK-MCS+U	2.037×10^{-3}	2.877	356.4	2.98
AK-MCS+EFF	1.958×10^{-3}	2.885	369.7	1.01
ABSVR1	1.955×10^{-3}	2.886	77.8	1.16
ABSVR2	1.951×10^{-3}	2.886	75.4	1.37

Note: The results of MCS, FORM, SORM, AK-MCS+U and AK-MCS+EFF are calculated using the UQLab [59].

other methods are illustrated in Table 5. It is observed from Table 5 that all the investigated methods give results with good agreement with the reference result, yet the converged solution of FORM and SORM require a higher number of functional calls than the adaptive surrogate methods. Among the adaptive algorithms, the AK-MCSi method exhibits the worst performance in terms of accuracy and efficiency, whereas the two proposed ABSVR approaches provide failure probability estimation with comparable accuracy as those of AK-IS and AK-ARBIS using much fewer functional calls. The results indicate that the proposed algorithm is well-suited for calculating extremely low failure probability when combined with the IS method. It is noteworthy that other advanced simulation approaches can also be integrated with the proposed algorithm for evaluating extremely low failure probabilities, which is a topic worth further exploring.

7.4. Example 4: A high dimensional problem

The fourth example considers a high-dimensional case, which is a typical benchmark problem in the structural reliability analysis that has been investigated in [26,62,65]. The performance function is given as:

$$G(\boldsymbol{x}) = n + 3\sigma\sqrt{n} - \sum_{i=1}^{n} x_i \tag{40}$$

where $x_i, i = 1, 2, \ldots, n$ are the independent random variables following the Lognormal distribution with means of $\mu = 1$ and standard deviations of $\sigma = 0.2$. In this example, the dimensionality n is taken as 40.

The reliability analysis results of ABSVR1 and ABSVR2 are compared with those of FORM, SORM, AK-MCS+U and AK-MCS+EFF, which are all summarized in Table 6. The reference result is calculated from MCS with a sample size of 1×10^6 and the corresponding failure probability is $\hat{P}_f = 1.978 \times 10^{-3}$ with a coefficient of variation smaller than 3%.

Table 6 shows that FORM underestimated the failure probability with a factor of almost 10 at the cost of 168 functional calls. Although SORM can largely improve the accuracy of FORM, yet the estimation error is still large, e.g. with a relative error of 26.09%, let alone the large functional calls of SORM for this particular case.

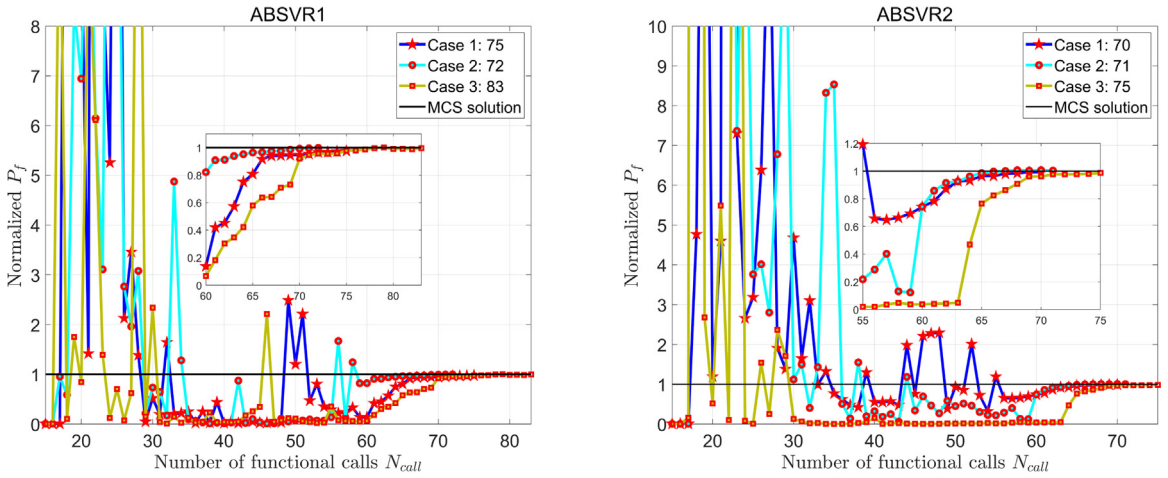

Fig. 15. The convergence history of failure probability: (a) The results of ABSVR1; (b) The results of ABSVR2. (For interpretation of the references to color in this figure, please refer to the web version of this article.)

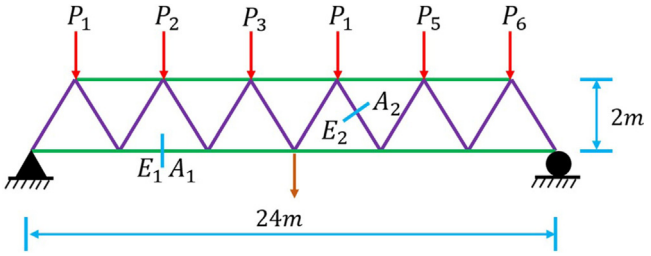

Fig. 16. A 2D truss structure.

The failure probability results provided by the investigated adaptive algorithms are all in close agreement with the MCS result, albeit the required computational effort varies among these methods. Specifically, the functional calls of AK-MCS+U and AK-MCS+EFF are much higher than those of ABSVR1 and ABSVR2, and a remarkable trade-off between accuracy and efficiency is achieved by the proposed algorithm for this high-dimensional case. The convergence history of failure probability by three independent runs of ABSVRs are depicted in Fig. 15, where the estimation results of ABSVR1 and ABSVR2 are seen to fluctuate significantly in the first 50 iterations before converged to the reference solution. Overall, the proposed algorithm provides a satisfactory estimation of failure probability at a lower cost than FORM for this high dimensional case. Nevertheless, the reliance on more efficient approaches such as dimension reduction techniques is rather necessary to more efficiently deal with extremely high dimensional problems.

7.5. Example 5: Reliability of a truss structure

To test the proposed algorithm on a more realistic engineering benchmark, a 2D truss structure as sketched in Fig. 16 is considered. There are 10 random variables involved in this structure, namely the cross-section and Young's modulus (A_1, E_1) of the horizontal bars, the cross-section and Young's modulus (A_2, E_2) of the diagonal bars and the six random loads $(P_1, P_2, \ldots, P_6)$. The distribution information of these random variables is given in Table 7. The response of interest is the displacement $\Delta(\boldsymbol{x})$ at the midspan, and the performance function of this truss structure is cast as [41]:

$$G(\boldsymbol{x}) = \Delta_t - |\Delta(\boldsymbol{x})| \tag{41}$$

Table 7
Statistical information of the random variables.

Random variable	Distribution	Mean	Standard deviation
A_1 (m^2)	Lognormal	2.0×10^{-3}	2.0×10^{-4}
A_2 (m^2)	Lognormal	1.0×10^{-3}	1.0×10^{-4}
E_1 (Pa)	Lognormal	2.1×10^{11}	2.1×10^{10}
E_2 (Pa)	Lognormal	2.1×10^{11}	2.1×10^{10}
$P_1, P_2, \ldots, P_6$ (N)	Gumbel	5.0×10^{4}	7.5×10^{3}

Table 8
Reliability analysis results for Example 4 using different methods.

Methods	$\hat{P}_f$	$\widehat{\beta}$	N_f	$\epsilon_{\hat{P}_f}$ (%)
MCS*	1.52×10^{-3}	2.96	1×10^{6}	–
FORM*	0.76×10^{-3}	3.17	160	50.00
SORM*	1.63×10^{-3}	2.94	372	7.24
AK-MCS*	1.52×10^{-3}	2.96	300	0.00
A-bPCE*	1.48×10^{-3}	2.97	129	2.63
ABSVR1	1.538×10^{-3}	2.961	57.8	1.18
ABSVR2	1.512×10^{-3}	2.965	54.9	0.53

Note: * Results reproduced from [41].

where $\Delta_t = 12$ cm is the critical threshold that ensures the structure operates in the nominal range. Since the structural displacement $\Delta(\boldsymbol{x})$ is implicitly defined in terms of the random variables, a finite element programme is adopted to calculate the value of $\Delta(\boldsymbol{x})$.

The results of failure probability estimation using various methods are summarized in Table 8, where the results of MCS, FORM, SORM, AK-MCS and A-bPCE are reproduced from [41]. One can see from Table 8 that FORM yields an erroneous result with a relative error as high as 50%, at the cost of 160 functional calls. Although SORM can notably improve the accuracy of FORM, the number of functional calls is seen to have increased significantly. The results of FORM and SORM suggest the nonlinearity of the underlying problem in the transformed standard normal space. As for the adaptive algorithms, the highest accuracy is achieved by AK-MCS (with the obtained failure probability the same as the reference one), yet at the expense of higher computational cost. On the contrary, both the ABSVR1 and ABSVR2 can provide results with comparable accuracy (slightly better) as that of A-bPCE using fewer functional calls, indicating the effectiveness of ABSVR to reach a balanced performance in terms of accuracy and efficiency. The convergence history of failure probability by three independent runs of ABSVRs are depicted in Fig. 17, where the estimation results of ABSVR1 and ABSVR2 are seen to quickly converge to the reference solution after significant fluctuation in the first 10 iterations. Moreover, for this case involving the finite element analysis and non-normal random variables, no embedded optimization algorithm nor iso-probabilistic transformation is required in the ABSVRs, which makes them easily implementable.

7.6. Example 6: A cantilever tube

The last example considers a cantilever tube as shown in Fig. 18. This tube is subjected to three external forces F_1, F_2, P and one torsion T, and will fail when the yield strength σ is smaller than the maximum stress $\sigma_{\max}$. Thus, the performance function can be expressed as [33,61]:

$$g(\boldsymbol{x}) = \sigma - \sigma_{\max} \tag{42}$$

where $\sigma_{\max}$ is the maximum von Mises stress of the tube and is calculated as:

$$\sigma_{\max} = \sqrt{\sigma_x^2 + 3\tau_{zx}^2} \tag{43}$$

where σ_x and τ_{zx} represent the normal stress and torsional stress on the top of surface of the tube at the origin, which are respectively given as:

$$\sigma_x = \frac{P + F_1 \sin\theta_1 + F_2 \sin\theta_2}{A} + \frac{Md}{2I} \tag{44}$$

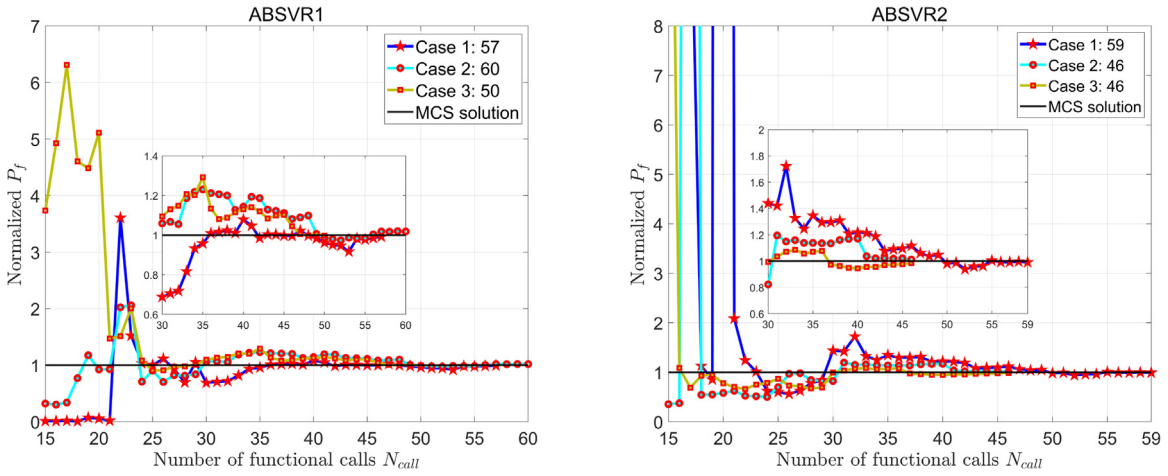

Fig. 17. The convergence history of failure probability: (a) The results of ABSVR1; (b) The results of ABSVR2. (For interpretation of the references to color in this figure, please refer to the web version of this article.)

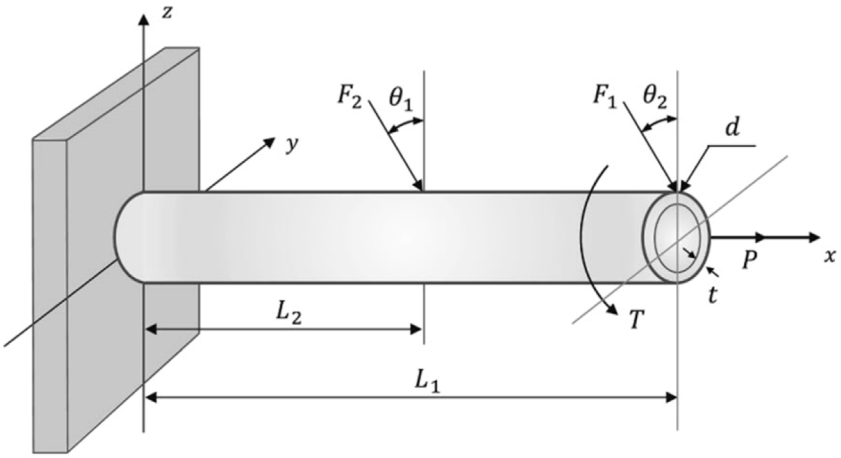

Fig. 18. A cantilever tube (after [61]).

$$\tau_{zx} = \frac{Td}{2J} \tag{45}$$

where A is the cross-sectional area, M denotes the bending moment and I represents the moment of inertia. These parameters can be calculated as:

$$M = F_1 L_1 \cos\theta_1 + F_2 L_2 \cos\theta_2 \tag{46}$$

$$A = \frac{\pi}{4}\left[d^2 - (d-2t)^2\right] \tag{47}$$

$$I = \frac{\pi}{64}\left[d^4 - (d-2t)^4\right] \tag{48}$$

$$J = 2I \tag{49}$$

A total of 9 random variables are involved in this example and their statistical information is listed in Table 9. The results of failure probability estimation using the proposed ABSVR1 and ABSVR2 along with other methods are

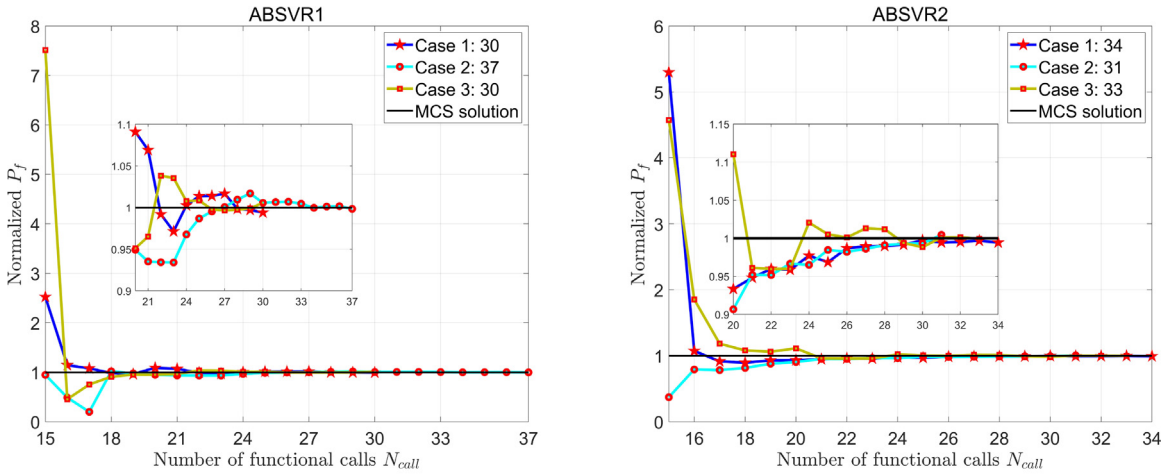

(a) (b)

Fig. 19. The convergence history of failure probability: (a) The results of ABSVR1; (b) The results of ABSVR2. (For interpretation of the references to color in this figure, please refer to the web version of this article.)

Table 9
Statistical information of the random variables.

Random variable	Distribution	Parameter 1	Parameter 2
t (mm)	Normal	5	0.1
d (mm)	Normal	42	0.5
L_1 (mm)	Uniform	119.75	120.25
L_2 (mm)	Uniform	59.75	60.25
F_1 (kN)	Normal	3	0.3
F_2 (kN)	Normal	3	0.3
P (kN)	Gumbel	27	2.7
T (N m)	Normal	90	9
σ (MPa)	Normal	220	22

Note: For uniform distribution, parameters 1 and 2 are the lower and upper bounds, respectively, while they represent the mean and standard deviation for Normal and Gumbel distributions.

summarized in Table 10, in which the results of AK-MCS+EFF, REAK and ISKRA (and their estimation errors) are directly taken from [33] and the results of FORM and SORM are calculated using the UQLab [59]. The reference result of this example is averaged over 10 independent runs of MCS with 1×10^6 sample points, giving the result of $\widehat{P}_f = 7.093 \times 10^{-3}$ with a coefficient of variation $\delta_{P_f} = 1.45\%$.

It is seen from Table 10 that, for this slightly nonlinear case, the result of FORM exhibits an error of 12.12%, whereas the results provided by other investigated methods are in good agreement with the reference one. It is noteworthy that due to different number of samples used in [33] and the present study, the reference results are a bit different, i.e. the coefficient of variation δ_{P_f} for MCS* with 6×10^4 samples is $\delta_{P_f} = 4.92\%$ and the one for MCS with 1×10^6 samples is $\delta_{P_f} = 1.18\%$. Nevertheless, the proposed ABSVR1 and ABSVR2 show a good trade-off between accuracy and efficiency for this case, i.e. reach a relative error within 0.5% with a functional call even less than that of FORM. The convergence history of failure probability by three independent runs of ABSVRs are depicted in Fig. 19, where the estimation results are seen to have quickly converged to the reference solution for both ABSVR1 and ABSVR2 after fluctuated significantly in the first 7 iterations.

8. Conclusions

In this paper, an adaptive algorithm based on Bayesian SVR (ABSVR) is proposed for efficient and accurate reliability analysis. According to the loss function employed to establish the BSVR model, two versions of ABSVR

Table 10
Reliability analysis results for Example 6 using different methods.

Methods	$\hat{P}_f$	$\widehat{\beta}$	N_f	$\epsilon_{\hat{P}_f}$ (%)
MCS*	6.850×10^{-3}	2.465	6×10^4	–
AK-MCS+EFF	6.850×10^{-3}	2.465	84	0
REAK	6.817×10^{-3}	2.467	59	0.49
ISKRA	6.850×10^{-3}	2.846	71	0
MCS	7.093×10^{-3}	2.453	1×10^6	–
FORM	6.233×10^{-3}	2.499	66	12.12
SORM	6.979×10^{-3}	2.458	239	1.61
ABSVR1	7.074×10^{-3}	2.453	31.9	0.27
ABSVR2	7.060×10^{-3}	2.454	31.2	0.47

Note: The reference result MCS* in [33] is obtained by MCS with a population size of 6×10^4, based on which the relative error of AK-MCS+EFF, REAK and ISKRA are calculated.

are proposed, namely the ABSVR1 based on square loss function and the ABSVR2 based on ε-insensitive square loss function. Following the concept of the penalty function method in optimization, a new learning function known as SLF is introduced for effective selection of informative sample points, e.g. points close to the limit state surface (LSS) in critical regions with sufficiently high probability density. To improve the uniformity of samples in the design of experiments, a distance constraint term is added to the learning function to control the density of samples. Besides, the adaptive sampling region scheme originally developed for Kriging-based approaches is adapted here to further enhance the computational efficiency by filtering out sample points with weak probability density, in that these samples have little contribution to the failure probability evaluation. Moreover, a hybrid error-based stopping criterion using the bootstrap confidence estimation is developed to terminate the active learning process to ensure that the learning algorithm stops at an appropriate stage.

To illustrate the performance of the proposed ABSVRs for structural reliability analysis, six numerical examples including one system reliability problem and four engineering cases are investigated, the results of which are compared to those from other state-of-the-art reliability methods. The results have shown that both the proposed ABSVR1 and ABSVR2 are well-suited for structural reliability analysis, and delivers failure probability estimation with better performance in terms of accuracy and efficiency than other methods considered. Besides, the proposed learning function exhibits excellent performance for guiding the search toward informative samples close to the LSS and thus, contributing to the fast convergence of the failure probability evaluation using the BSVR model.

Overall, the proposed ABSVR is easy to implement since no embedded optimization algorithm nor iso-probabilistic transformation is required, and its applicability and effectiveness for structural reliability analysis have been validated through numerical examples featuring different levels of complexity. However, this work is still an early step towards applying Bayesian SVR for reliability analysis of complex engineering structures, the integration of ABSVR with more advanced simulation methods (e.g. the subset simulation) and dimension reduction techniques (e.g. the principle of component analysis) is worth exploring to deal with rare failure events and/or extremely high-dimensional problems.

Declaration of competing interest

The authors declare that they have no known competing financial interests or personal relationships that could have appeared to influence the work reported in this paper.

Acknowledgments

The financial support for this study was provided in part by the National Natural Science Foundation of China (No. 52078425) and Ahsan Kareem was supported in part by the Robert M. Moran Professorship. This support is highly appreciated. All the opinions presented here are those of the writers, not necessarily represent those of the sponsors.

References

[1] Jie Li, Jianbing Chen, Stochastic Dynamics of Structures, John Wiley & Sons, 2009.
[2] J.-M. Bourinet, Rare-event probability estimation with adaptive support vector regression surrogates, Reliab. Eng. Syst. Saf. 150 (2016) 210–221.
[3] Nicolas Lelièvre, Pierre Beaurepaire, Cécile Mattrand, Nicolas Gayton, AK-MCSi: A Kriging-based method to deal with small failure probabilities and time-consuming models, Struct. Saf. 73 (2018) 1–11.
[4] Nolan Kurtz, Junho Song, Cross-entropy-based adaptive importance sampling using Gaussian mixture, Struct. Saf. 42 (2013) 35–44.
[5] Iason Papaioannou, Costas Papadimitriou, Daniel Straub, Sequential importance sampling for structural reliability analysis, Struct. Saf. 62 (2016) 66–75.
[6] Siu-Kui Au, James L. Beck, Estimation of small failure probabilities in high dimensions by subset simulation, Probab. Eng. Mech. 16 (4) (2001) 263–277.
[7] Ziqi Wang, Marco Broccardo, Junho Song, Hamiltonian Monte Carlo methods for Subset Simulation in reliability analysis, Struct. Saf. 76 (2019) 51–67.
[8] R.H. Lopez, A.J. Torii, L.F.F. Miguel, J.E. Souza Cursi, Overcoming the drawbacks of the FORM using a full characterization method, Struct. Saf. 54 (2015) 57–63.
[9] Shun-Peng Zhu, Behrooz Keshtegar, Subrata Chakraborty, Nguyen-Thoi Trung, Novel probabilistic model for searching most probable point in structural reliability analysis, Comput. Methods Appl. Mech. Engrg. 366 (2020) 113027.
[10] Armen Der Kiureghian, Hong-Zong Lin, Shyh-Jiann Hwang, Second-order reliability approximations, J. Eng. Mech. 113 (8) (1987) 1208–1225.
[11] Xianzhen Huang, Yuxiong Li, Yimin Zhang, Xufang Zhang, A new direct second-order reliability analysis method, Appl. Math. Model. 55 (2018) 68–80.
[12] Jinsheng Wang, Muhannad Aldosary, Song Cen, Chenfeng Li, Hermite polynomial normal transformation for structural reliability analysis, Eng. Comput. (2021).
[13] Muhannad Aldosary, Jinsheng Wang, Chenfeng Li, Structural reliability and stochastic finite element methods: State-of-the-art review and evidence-based comparison, Eng. Comput. 35 (6) (2018) 2165–2214.
[14] U. Bucher, A fast and efficient response surface approach for structural reliability problems, Struct. Multidiscip. Optim. 7(1) (1990) 57–66.
[15] Géraud Blatman, Bruno Sudret, Adaptive sparse polynomial chaos expansion based on least angle regression, J. Comput. Phys. 230 (6) (2011) 2345–2367.
[16] Maliki Moustapha, Jean-Marc Bourinet, Benoît Guillaume, Bruno Sudret, Comparative study of Kriging and support vector regression for structural engineering applications, ASCE-ASME J. Risk Uncertain. Eng. Syst. A 4 (2) (2018) 04018005.
[17] Jing Zhao, Chen Jianqiao, Li Xu, RBF-GA: An adaptive radial basis function metamodeling with genetic algorithm for structural reliability analysis, Reliab. Eng. Syst. Saf. 189 (2019) 42–57.
[18] Hyeongjin Song, Kyung K Choi, Ikjin Lee, Liang Zhao, David Lamb, Adaptive virtual support vector machine for reliability analysis of high-dimensional problems, Struct. Multidiscip. Optim. 47 (4) (2013) 479–491.
[19] Atin Roy, Subrata Chakraborty, Support vector regression based metamodel by sequential adaptive sampling for reliability analysis of structures, Reliab. Eng. Syst. Saf. (2020) 106948.
[20] A.M. Gomes, Comparison of response surface and neural network with other methods for structural reliability analysis, Struct. Saf. 26(1) (2004) 49–67.
[21] Kai Cheng, Zhenzhou Lu, Structural reliability analysis based on ensemble learning of surrogate models, Struct. Saf. 83 (2020) 101905.
[22] Zhili Sun, Jian Wang, Rui Li, Cao Tong, LIF: A new Kriging based learning function and its application to structural reliability analysis, Reliab. Eng. Syst. Saf. 157 (Complete) (2017) 152–165.
[23] Xu Li, Chunlin Gong, Liangxian Gu, Wenkun Gao, Zhao Jing, Hua Su, A sequential surrogate method for reliability analysis based on radial basis function, Struct. Saf. 73 (2018) 42–53.
[24] Zhengliang Xiang, Jiahui Chen, Yuequan Bao, Hui Li, An active learning method combining deep neural network and weighted sampling for structural reliability analysis, Mech. Syst. Signal Process. 140 (2020) 106684.
[25] B.J. Bichon, M.S. Eldred, L.P. Swiler, S. Mahadevan, J.M. Mcfarland, Efficient global reliability analysis for nonlinear implicit performance functions, Aiaa J. 46 (10) (2008) 2459–2468.
[26] B. Echard, N. Gayton, M. Lemaire, AK-MCS: An active learning reliability method combining Kriging and Monte Carlo simulation, Struct. Saf. 33 (2) (2011) p.145–154.
[27] Hongzhe Dai, Hao Zhang, Wei Wang, Guofeng Xue, Structural reliability assessment by local approximation of limit state functions using adaptive Markov chain simulation and support vector regression, Comput.-Aided Civ. Infrastruct. Eng. 27 (9) (2012) 676–686.
[28] J.M. Bourinet, Rare-event probability estimation with adaptive support vector regression surrogates, Reliab. Eng. Syst. Saf. 150 (2016) 210–221.
[29] Qiujing Pan, Daniel Dias, An efficient reliability method combining adaptive support vector machine and Monte Carlo simulation, Struct. Saf. 67 (2017) 85–95.
[30] Xufang Zhang, Lei Wang, John Dalsgaard Sorensen, REIF: A novel active-learning function toward adaptive Kriging surrogate models for structural reliability analysis, Reliab. Eng. Syst. Saf. 185 (may) (2019) 440–454.
[31] Yan Shi, Zhenzhou Lu, Ruyang He, Yicheng Zhou, Siyu Chen, A novel learning function based on Kriging for reliability analysis, Reliab. Eng. Syst. Saf. 198 (2020) 106857.
[32] Z. Wang, A. Shafieezadeh, ESC: an efficient error-based stopping criterion for Kriging-based reliability analysis methods, Struct. Multidiscip. Optim. 59(5) (2019) 1621–1637.

[33] Zeyu Wang, Abdollah Shafieezadeh, REAK: Reliability analysis through error rate-based adaptive Kriging, Reliab. Eng. Syst. Saf. 182 (2019) 33–45.
[34] Jiaxiang Yi, Qi Zhou, Yuansheng Cheng, Jun Liu, Efficient adaptive Kriging-based reliability analysis combining new learning function and error-based stopping criterion, Struct. Multidiscip. Optim. (2020) 1–20.
[35] B. Echard, N. Gayton, M. Lemaire, N. Relun, A combined importance sampling and Kriging reliability method for small failure probabilities with time-demanding numerical models, Reliab. Eng. Syst. Saf. 111 (2013) 232–240.
[36] Jingwen Song, Pengfei Wei, Marcos Valdebenito, Michael Beer, Adaptive reliability analysis for rare events evaluation with global imprecise line sampling, Comput. Methods Appl. Mech. Engrg. 372 (2020) 113344.
[37] Maijia Su, Guofeng Xue, Dayang Wang, Yongshan Zhang, Yong Zhu, A novel active learning reliability method combining adaptive Kriging and spherical decomposition-MCS (AK-SDMCS) for small failure probabilities, Struct. Multidiscip. Optim. (2020) 1–23.
[38] Tayyab Zafar, Yanwei Zhang, Zhonglai Wang, An efficient Kriging based method for time-dependent reliability based robust design optimization via evolutionary algorithm, Comput. Methods Appl. Mech. Engrg. 372 (2020) 113386.
[39] Zeng Meng, Zhuohui Zhang, Dequan Zhang, Dixiong Yang, An active learning method combining Kriging and accelerated chaotic single loop approach (AK-ACSLA) for reliability-based design optimization, Comput. Methods Appl. Mech. Engrg. 357 (2019) 112570.
[40] Rui Teixeira, Maria Nogal, Alan O'Connor, Adaptive approaches in metamodel-based reliability analysis: A review, Struct. Saf. 89 (2021) 102019.
[41] Stefano Marelli, Bruno Sudret, An active-learning algorithm that combines sparse polynomial chaos expansions and bootstrap for structural reliability analysis, Struct. Saf. 75 (2018) 67–74.
[42] Linxiong Hong, Huacong Li, Kai Peng, A combined radial basis function and adaptive sequential sampling method for structural reliability analysis, Appl. Math. Model.90, 375–393.
[43] W.L. Buntine, A.S. Weigend, Bayesian back-propagation, Complex Syst. 5 (6) (1991) 603–643.
[44] David J.C. MacKay, A practical Bayesian framework for backpropagation networks, Neural Comput. 4 (3) (1992) 448–472.
[45] Radford M. Neal, Bayesian Training of Backpropagation Networks by the Hybrid Monte carlo Method, Technical report, Citeseer, 1992.
[46] Peter Sollich, Bayesian methods for support vector machines: Evidence and predictive class probabilities, Mach. Learn. 46 (1) (2002) 21–52.
[47] James Tin-Yau Kwok, The evidence framework applied to support vector machines, IEEE Trans. Neural Netw. 11 (5) (2000) 1162–1173.
[48] Martin H.C. Law, James Tin-Yau Kwok, Bayesian support vector regression, in: International Workshop on Artificial Intelligence and Statistics, PMLR, 2001, pp. 162–167.
[49] Junbin B Gao, Steve R. Gunn, Chris J. Harris, Martin Brown, A probabilistic framework for SVM regression and error bar estimation, Mach. Learn. 46 (1) (2002) 71–89.
[50] Wei Chu, S. Sathiya Keerthi, Chong Jin Ong, Bayesian support vector regression using a unified loss function, IEEE Trans. Neural Netw. 15 (1) (2004) 29–44.
[51] Kai Cheng, Zhenzhou Lu, Active learning bayesian support vector regression model for global approximation, Inform. Sci. 544 (2021) 549–563.
[52] Kai Cheng, Zhenzhou Lu, Adaptive Bayesian support vector regression model for structural reliability analysis, Reliab. Eng. Syst. Saf. 206 (2021) 107286.
[53] Zhixun Wen, Haiqing Pei, Hai Liu, Zhufeng Yue, A sequential Kriging reliability analysis method with characteristics of adaptive sampling regions and parallelizability, Reliab. Eng. Syst. Saf. 153 (2016) 170–179.
[54] Alex J Smola, Bernhard Schölkopf, Klaus-Robert Müller, The connection between regularization operators and support vector kernels, Neural Netw. 11 (4) (1998) 637–649.
[55] M. Moustapha, C. Lataniotis, S. Marelli, B. Sudret, UQLab user Manual – Support Vector Machines for Regression, Report UQLab, V1.4–111, Chair of Risk, Safety and Uncertainty Quantification, ETH Zurich, Switzerland, 2021.
[56] Jean-Marc Bourinet, Reliability Analysis and Optimal Design Under Uncertainty-Focus on Adaptive Surrogate-Based Approaches (Ph.D. thesis), Université Clermont Auvergne, 2018.
[57] Xufang Zhang, Lei Wang, John Dalsgaard Sørensen, AKOIS: an adaptive Kriging oriented importance sampling method for structural system reliability analysis, Struct. Saf. 82 (2020) 101876.
[58] C. Lataniotis, S. Marelli, B. Sudret, UQLab user Manual–The Input Module, Report No. UQLab-V1, Chair of Risk, Safety and Uncertainty Quantification, ETH Zurich, Zurich, Switzerland, 2015, pp. 2–102.
[59] S. Marelli, R. Schöbi, B. Sudret, UQLab user Manual–Structural Reliability (Rare Event Estimation), Report UQLab-V0, 2016, pp. 9–107, Structural Reliability.
[60] Luc Schueremans, Dionys Van Gemert, Benefit of splines and neural networks in simulation based structural reliability analysis, Struct. Saf. 27 (3) (2005) 246–261.
[61] Jungho Kim, Junho Song, Probability-Adaptive Kriging in n-Ball (PAK-Bn) for reliability analysis, Struct. Saf. 85 (2020) 101924.
[62] Zeng Meng, Zhuohui Zhang, Gang Li, Dequan Zhang, An active weight learning method for efficient reliability assessment with small failure probability, Struct. Multidiscip. Optim. 61 (3) (2020) 1157–1170.
[63] Chunlong Xu, Weidong Chen, Jingxin Ma, Yaqin Shi, Shengzhuo Lu, AK-MSS: An adaptation of the AK-MCS method for small failure probabilities, Struct. Saf. 86 (2020) 101971.
[64] Wanying Yun, Zhenzhou Lu, Xian Jiang, Leigang Zhang, Pengfei He, AK-ARBIS: an improved AK-MCS based on the adaptive radial-based importance sampling for small failure probability, Struct. Saf. 82 (2020) 101891.
[65] Tong Zhou, Yongbo Peng, Structural reliability analysis via dimension reduction, adaptive sampling, and Monte Carlo simulation, Struct. Multidiscip. Optim. (2020) 1–23.